U(VI) and Th(IV) recovery using silica beads functionalized with urea- or thiourea-based polymers – Application to ore leachate

Mohammed Hamza, Yuezhou Wei, Mahmoud Khalafalla, Neveen Abed, Amr Fouda, Khalid Elwakeel, Eric Guibal, Nora Hamad

U(VI) and Th(IV) recovery using silica beads functionalized with urea- or thiourea-based polymers – Application to ore leachate

Mohammed F. Hamza [a,b], Yuezhou Wei [a,c,*], Mahmoud S. Khalafalla [b], Neveen S. Abed [b], Amr Fouda [d], Khalid Z. Elwakeel [e,f], Eric Guibal [g,*], Nora A. Hamad [h]

[a] School of Nuclear Science and Technology, University of South China, Heng Yang 421001, China
[b] Nuclear Materials Authority, POB 530, El-Maadi, Cairo, Egypt
[c] School of Nuclear Science and Engineering, Shanghai Jiao Tong University, Shanghai, China
[d] Botany and Microbiology Department, Faculty of Science, Al-Azhar University, Nasr City, Cairo 11884, Egypt
[e] University of Jeddah, College of Science, Department of Chemistry, Jeddah, Saudi Arabia
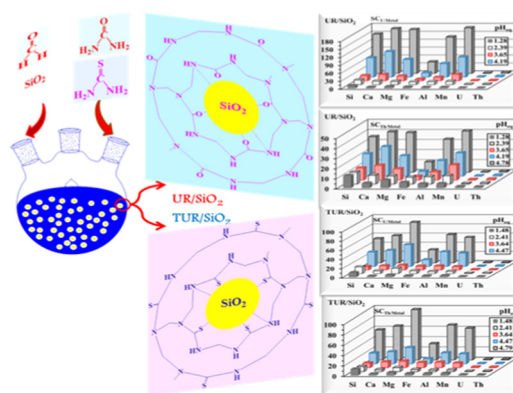[f] Environmental Science Department, Faculty of Science, Port-Said University, Port-Said, Egypt
[g] Polymers Composites and Hybrids (PCH), IMT Mines Ales, Alès, France
[h] Faculty of Science, Menoufia University, Shebine El-Koam, Egypt

HIGHLIGHTS

- Efficient functionalization of silica beads by formaldehyde-crosslinked urea.
- U(VI) and Th(IV) maximum sorption capacities ~1–1.2 mmol g^{-1}, at pH 5.
- Uptake kinetics fitted by the pseudo-first order rate.
- Efficient metal desorption with HCl solutions; stability at sorbent recycling.
- A flowsheet is proposed for selective recovery of U(VI) and Th(IV).

GRAPHICAL ABSTRACT

ABSTRACT

Urea and thiourea have been successfully deposited at the surface of silica beads (through one-pot reaction with formaldehyde) for designing new sorbents for U(VI) and Th(IV) recovery (UR/SiO$_2$ and TUR/SiO$_2$ composites, respectively). These materials have been characterized by FTIR, titration, elemental analysis, BET, TGA, SEM-EDX for identification of structural and chemical properties, and interpretation of binding mechanisms. Based on deprotonation of reactive groups (amine, carbonyl, or thiocarbonyl) and metal speciation, the optimum pH was ~4. Uptake kinetics was fast (equilibrium within 60–90 min). Although the kinetic profiles are fitted by the pseudo-first order rate equation, the resistance to intraparticle diffusion cannot be neglected. Sorption isotherms were fitted by Langmuir equation (maximum sorption capacities: 1–1.2 mmol g^{-1}). Thermodynamics are also investigated showing differences between the two types of functionalized groups: exothermic for TUR/SiO$_2$ and endothermic for UR/SiO$_2$. Metal desorption is highly effective using 0.3–0.5 M HCl solutions: total desorption occurs within 30–60 min; sorption/desorption properties are remarkably stable for at least 5 cycles. The sorbents have marked preference for U(VI) and Th(IV)

* Corresponding authors.
E-mail addresses: m_fouda21@hotmail.com (M.F. Hamza), yzwei@sjtu.edu.cn (Y. Wei), mahmoudsayed24@yahoo.com (M.S. Khalafalla), nova848@yahoo.com (N.S. Abed), amr_fh83@azhar.edu.eg (A. Fouda), kelwkeel@uj.edu.sa (K.Z. Elwakeel), eric.guibal@mines-ales.fr (E. Guibal), nhamad059@gmail.com (N.A. Hamad).

over alkali-earth and base metals at pH_{eq} ~4.8. By preliminary precipitation steps, it is possible "cleaning" ore leachates of pegmatite ore, and recovering U(VI) and Th(IV) using functionalized silica beads. After elution and selective recovery by precipitation with oxalate (Th-cake) and alkaline (U-cake), the metals can be valorized.

1. Introduction

The development of new sorbents and new sorption processes is driven by dual strong incentives at national and international levels such as: (a) the necessity to minimize the impact of industrial activity on the environment (including water body compartment) (Rosenberg et al., 2016; Xie et al., 2019), and (b) the development of recycling strategies (to save primary resources, optimize global uses, and promote independent sourcing of strategic targets) (Sun et al., 2016; Swain and Mishra, 2019). Metal ions are important contributors to the contamination of water bodies due to the discharge of industrial wastewater containing hazardous contaminants (which are accumulative in the food chain and may have high toxicological impact) (Bleise et al., 2003; Zhang et al., 2011). The high demand on metals for high-tech applications (for example, rare earth elements, REEs) (Swain and Mishra, 2019), the high tension on base and precious metals made strategic the development of processes for recovering these metals from secondary sources (tailings, industrial wastes, or sub-marginal ores) (Wu et al., 2017). The nuclear power industry requires the supply of uranium, which is frequently associated with thorium in most geological resources (Gabriel et al., 2013).

In most cases, the first step in the recovery process from these mineral or material resources consists of leaching steps (Abhilash and Pandey, 2013; Zhang et al., 2016), followed by concentration and separation processes, such as solvent extraction (Wu et al., 2018) (including extractant impregnated sorbents (Mosleh et al., 2020), and membranes), precipitation (Borai et al., 2016; Hamza et al., 2019) (eventually coupled to bioreduction, (You et al., 2021)). The sorption of uranium was investigated using different types of sorbents such as ion exchange resins (Ang et al., 2017; Smirnov et al., 2017), chelating resins (Ang et al., 2018; Zidan et al., 2020), mineral sorbents (Gladysz-Plaska et al., 2018; Liao et al., 2019), biosorbents (Dabbagh et al., 2018; Hamza et al., 2021; Nuhanovic et al., 2019; Ozudogru and Merdivan, 2020), biobased char (Ahmed et al., 2021), or iron-based materials (Chen et al., 2017). Composite materials (Liu et al., 2020b; Yilmaz et al., 2020) (Kamal et al., 2021; Liu et al., 2021a; Liu et al., 2021b) (Wang et al., 2021), and metal-organic frameworks (Li et al., 2021) have also retained a great attention requiring frequently complex synthesis methods.

Apart the proper reactivity of OH groups at the surface of SiO_2, these materials are very efficient for elaborating composite sorbents; indeed, silica particles and beads bring useful stable mechanical properties and highly porous characteristics. In addition, the specific porosity of silica may contribute to expand the specific surface area of polymer-based composites. The functionalization of these surfaces allows increasing the reactivity and selectivity of these sorbents. A wide diversity of functional groups have been immobilized at the surface of silica-based supports, including amino-acids (Ismail et al., 2020; Yang et al., 2018), amino-compounds (Amesh et al., 2020b; Hamza, 2019; Wamba et al., 2018), organic acids (Amesh et al., 2020a; Kouraim et al., 2019), phosphorous-based moieties (Giannakoudakis et al., 2021; Guo et al., 2017; Sarafraz et al., 2017; Yang et al., 2019), sulfonic groups (El-Magied et al., 2018), amidoxime groups (Xiao et al., 2018; Yin et al., 2017; Yin et al., 2015), cyclodextrin and macrocycles (Barbette et al., 2004; Liu et al., 2016).

Urea- and thiourea-based sorbents have been successfully used for the sorption of uranium or thorium. These functional groups were grafted on biopolymers such as chitosan (Orabi et al., 2018; Wang et al., 2020), cellulose (Orabi, 2019), or their derivatives impregnated in synthetic resin (such as Amberlite XAD-16) (Merdivan et al., 2001). Urea-formaldehyde (Ertan and Guelfen, 2009; Kirci et al., 2009) and thiourea-formaldehyde (Gezer et al., 2011; Muslu and Gulfen, 2011) (Elwakeel et al., 2020; Hao et al., 2014) resins have already shown their interest in sorption applications. Urea-formaldehyde resin (synthesized as micron-size particles) were also

directly used for uranium recovery (Hao et al., 2014; Ma et al., 2020): sorption reached an optimum at pH 5–6 with equilibrium time close to 180–240 min and a maximum sorption capacity around 0.42 mmol U g^{-1}. There is a need for developing simple synthesis procedures for elaborating highly reactive composite materials having good mechanical stability, fast kinetics of sorption and good regeneration properties.

The complementary properties of silica-based materials (mechanical and textural characteristics) and urea/thiourea reactivity (amino- and thio-based groups) clearly highlight the potential interest of directly grafting urea-based compounds on silica supports. A very simple process is applied in this work for the coating of silica beads by the condensation of urea or thiourea at the surface of the material using formaldehyde as the crosslinking agent in acidic solution. Depositing the functionalized polymers as a thin layer at the surface of silica beads is supposed to offer several advantages such as higher mechanical stability, and both higher accessibility and availability of reactive groups (specific surface area), compared with bulk polymer (including improvement of mass transfer properties).

The urea-formaldehyde resins have been investigated for metal binding (including uranyl removal) showing some limitations in terms of mass transfer and sorption performances (maximum sorption capacities). Herein, the concept is based on the association of a stable mechanical core (silica) with a polymer coating (shorter diffusion layer for enhanced mass transfer). The coating layer allows producing micro-size objects that can be efficiently separated by settling and sieving (contrary to nanometer sizes that would be required for single urea-formaldehyde resins for reaching short equilibrium times). In addition, the second objective of this work consisted in evaluating the beneficial/antagonist effect of substituting urea with thiourea in terms of sorption performances and binding mechanisms. This concept is relatively simple (one-pot coating step on pre-formed silica beads) not involving complex modifications or sophisticated supports as may consist when functionalization steps are required or when using for example metal organic framework. Another benefit of this study consists of the testing of the process with real effluents (an aspect frequently underestimated).

In this study, the sorption properties of urea- and thiourea-functionalized silica beads (UR/SiO_2 and TUR/SiO_2 respectively) are compared for the recovery of both U(VI) and Th(IV), first from synthetic solutions, before applying the sorbents to the treatment of pre-treated pegmatite-ore leachates.

2. Materials and methods

2.1. Materials

Thiourea, urea, acetic acid, and formaldehyde solution (ACS reagent 37% w/w) were purchased from Sigma-Aldrich (Merck, Darmstadt, Germany). Silica particles were obtained from Asahi Chemicals, Co Ltd., Osaka (Japan). Uranyl nitrate hexahydrate ($UO_2(NO_3)_2 \cdot 6H_2O$) was supplied by SPI Supplies (West Chester, PA, USA). Acetone was purchased from Chron Chemicals (Qionglai, China). Thorium nitrate hydrate (Th$(NO_3)_4 \cdot xH_2O$) was obtained from Otto Chemie Pvt. Ltd. (Popatwadi, Mumbai India). Bromofom was supplied by Adwic (Qaliubiya, Egypt). Other chemicals were purchased from Prolabo products (VWR, Avantor Group, Fontenay-sous-Bois France). Reagents were used as received (reagent grade).

2.2. Synthesis procedures

For the synthesis of UR/SiO_2 and TUR/SiO_2, 7.2 g of Urea (UR) or Thiourea (TUR) were dissolved in 20 mL of demineralized water, respectively.

The solution was transferred into a 100-mL round bottom flask (equipped with a condenser); 10 g of silica were introduced in the reactor. Formaldehyde (37% *w*/w aqueous solution; 7.2 mL) was added into the reactor, the pH of the suspension was turned to acidic medium (pH close to 3) by using glacial acetic acid (1 mL). The mixture was refluxed at 90 $\pm$ 3 °C, under vigorous agitation, for 5 h. The white precipitate was collected by filtration and rinsed with acetone, before being air-dried at 60 °C overnight. The final product for both UR/SiO$_2$ and TUR/SiO$_2$ weighted ~18.9 g; this means a grafting yield of ~95%. The synthesis route is illustrated by Scheme 1. The synthesis of sorbents took place in water system instead of solvent to avoid the use of hazardous solvents and decreasing the synthesis cost. The polymerization reaction was operated under air atmosphere. The yield of grafting was determined through the average ratio of the total weight of the final polymers and the weight of reagents (monomers, reagents, etc.). This interaction is supposed to proceed through the reactive surface of silica beads via the interaction of hydrophilic groups present on the polymer composite. This was reported in previous work for the grafting of amine moieties on mesoporous silica. This hypothesis is based on the possibility of siloxyl groups on the silica surface to be coupled with various hydrophilic agents as monomers and functional groups without processing surface pre-functionalization.
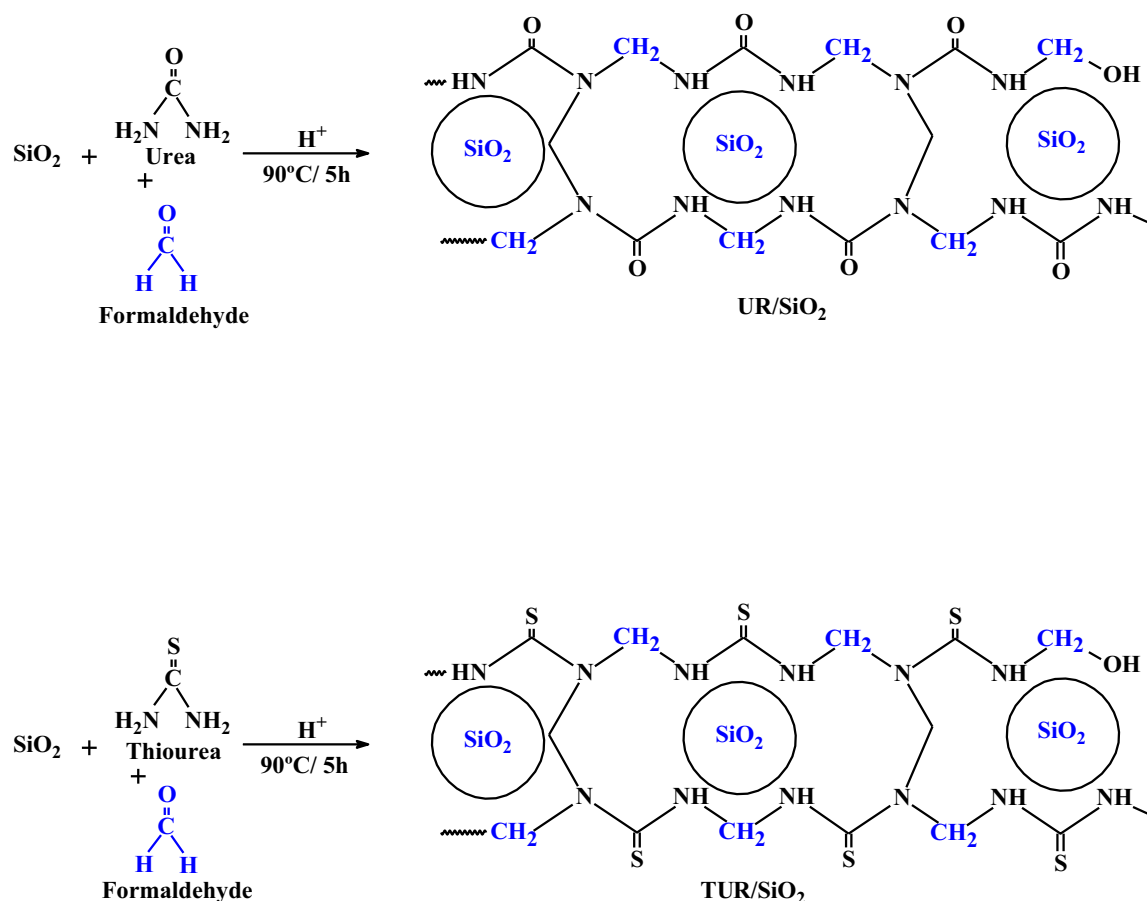
2.3. Characterization of materials

FT-IR spectra were acquired using a Shimadzu-IRTracer-100 FT-IR spectrometer (Shimadzu Instruments, Tokyo, Japan). The samples (dried at 60 °C) were grinded and mixed with KBr (1%, *w*/w) before being pressed to form compact KBr discs for FTIR transmission analysis. The C, O, H, S, and N contents were determined using a 2400 Series II CHNS/O elemental analyzer (Perkin-Elmer, Waltham, MA, USA). The thermogravimetric analysis was performed using a TG-DTA Netzsch STA 449 F3 Jupiter equipment (NETZSCH-Gerätebau, GmbH, Selb, Germany) under N$_2$ atmosphere. The morphology of composite sorbents was characterized by scanning electron microscopy (SEM) using a Phenom ProX (Thermo Fisher Scientific, Eindhoven-Netherlands), while the semi-quantitative surface analyses were achieved by energy dispersive X-ray analysis (integrated to Phenom ProX SEM). The textural properties of silica particles, before and after functionalization, were measured using the BJH method. The samples were degassed at 120 °C for 12 h before being analyzed using a Micromeritics TrisStar II surface area and porosity analyzer (Micromeritics Instrument Corporation, Norcross, GA, USA). The analysis of the global surface charge of the sorbents was performed by the determination of their pH$_{PZC}$ using the pH-drift method (Lopez-Ramon et al., 1999). A fixed amount of sorbent (i.e., ~100 mg) was dispersed into a series of flasks containing 50 mL of an aqueous solution (background salt: NaCl, 0.1 M), with initial pH value (pH$_0$) varying between 1 and 14. The equilibrium pH (pH$_{eq}$) was monitored after 48 h of agitation (using a pH-26A pH-meter, Acculab, New York, USA). The pH$_{PZC}$ value corresponds to the pH respecting pH$_0$ = pH$_{eq}$.

2.4. Sorption tests

Sorption tests were carried out in batch systems. The solution (*V*, L) containing a fixed metal concentration (*C*$_0$, mmol L^{-1}) at pH$_0$ was mixed with a given amount of sorbent (*m*, g) under agitation (velocity: 210 rpm), at room temperature (*T*: 22 $\pm$ 1 °C) for 48 h. Samples were collected and filtrated. The residual concentrations (*C*$_{eq}$, mmol L^{-1}) for individual metal ions were determined using ICP-AES analysis (ICPS-7510, Shimadzu, Kyoto, Japan). For uptake kinetics, samples were homogeneously withdrawn at given contact times, filtrated, and analyzed. The

Scheme 1. Synthesis procedures and proposed structures of UR/SiO$_2$ and TUR/SiO$_2$ sorbents.

sorption capacity (q_{eq}, mmol g^{-1}) was deduced from the mass balance equation: $q_{eq} = (C_0 - C_{eq}) \times V/m$. These experimental conditions were individually fixed in function of their specific objectives. Specific and detailed experimental conditions are reported in the caption of all figures (see below).

The uptake kinetics were fitted with the pseudo-first and pseudo-second order rate equations (PFORE and PSORE, respectively), and the model of resistance to intraparticle diffusion (RIDE, the so-called Crank equation) (Table S1a, see Supplementary Information). For equilibrium experiments, the Langmuir, Freundlich, and Sips equations were used for modeling sorption isotherms (Table S1b). For sorption in multi-component solutions, the same procedures were applied; the combined solution was prepared with equimolar concentrations of metal/metalloid ions (1 mmol L^{-1}) at pH 5 (before adjusting the pH to several lower values for investigating the impact of pH on selectivity).

Metal desorption was operated using similar experimental procedures for desorption kinetics, and metal desorption/sorbent recycling steps (water rinsing step was operated between each sorption/desorption runs). Metal-loaded sorbents were collected from uptake kinetic series. The mass balance equation was used for calculating the sorption efficiency and capacity as well as the desorption efficiency. Different eluents were tested, including 1 M NaCl/0.1 M H$_2$SO$_4$, 0.5 M HNO$_3$, 1 M citric acid, and 1 M Na$_2$CO$_3$.

Experiments were systematically duplicated; duplicated experimental profiles are reported for illustrating the good reproducibility of results (preferentially to presenting average values and error bars).

2.5. Ore leaching and metal recovery

The characteristics of the ore (geological and mineralogical information) are documented in Annex A (see Supplementary Information). The pegmatite material was collected from the Abu Rusheid zone in the South Eastern Desert Egyptian district. The analysis of metal content in the ore sample was performed after dissolving, using a series of different acids. A fixed amount (i.e., 0.5 g) of quartered ore sample was digested in a Teflon beaker (at 120–150 °C) using HF concentrated acid (10 mL) for Si digestion. After evaporation of HF, a mixture of HNO$_3$ (10 mL) and HCl (10 mL) concentrated acids was added under continuous heating for dissolving the mineral residue; a few drops of H$_2$O$_2$ were also added for dissolving organic matter. Filtrated solution was diluted using 100-mL measuring flask for analysis of trace and major elements. Uranium was determined using the ammonium metavanadate method (Davies and Gray, 1964; Mathew et al., 2009) and Arsenazo method for REE analysis (Marczenko and Balcerzak, 2000) by spectrophotometric determination using a UV spectrophotometer (UV-160, Shimadzu, Kyoto, Japan) at the wavelength: 654 nm. Other elements in the leaching solution were measured using a Unicam 969 atomic absorption spectrometer (Thermo Electron Corporation, Waltham, MA, USA).

The mineralogical composition of the ore after grinding, sieving, and bromofom separation is reported in Table S2. The acidic leaching was operated by contact of grinded ore with sulfuric acid (200 g L^{-1}, ~2 M) under agitation (v: 200 rpm) for 2 h, at T: 22 ± 3 °C. The solid/liquid ratio was set to 1:3 (i.e., 1 kg for 3 L of acidic leaching solution). Under these conditions, U and Th elements are partially leached (see below); however, these mild conditions have been selected for minimizing the dissolution of most rare metals such as Hf, Ta, and Zr (their recovery is currently under development).

The high contents of Fe and Al in the ore induce high relative concentrations of these two metals in the acidic leachates (pregnant liquor solution, PLS, 2.4 L). To avoid excessive competition for further sorption tests, the pH of the leachates was successively adjusted to pH 4 and pH 5 with NaOH to sequentially precipitate Fe and Al and produce pre-treated (precipitated) pregnant liquor solution (PPLS).

Sorption tests were performed on PPLS using both UR/SiO$_2$ and TUR/SiO$_2$, at different pH values (i.e., pH$_{eq}$: 1.28, 2.39, 3.65, 4.19, and 4.78 for UR/SiO$_2$ and pH$_{eq}$: 1.48, 2.41, 3.64, 4.47, and 5.79 for TUR/SiO$_2$).

The sorbent dose, SD, was 5 g L^{-1} and the contact time was set to 5 h (agitation: 210 rpm; T: 22 ± 1 °C).

Metal desorption was operated using 0.5 M HCl solutions with a sorbent dose of 17 g L^{-1} at T: 22 ± 3 °C for 60-min stirring time, at v: 120 rpm.

The eluates were treated by precipitation:

(a) First, at pH ~1, with oxalic acid solution (20% w/w; i.e., ~2.2 mol L^{-1}); 20 mL oxalate solution per 100 mL of eluate, at T: 22 ± 3 °C, under stirring (30 min), for the precipitation of thorium oxalate cake (Kursunoglu et al., 2021).
(b) Finally, at pH 8 (controlled with NaOH solution) for the precipitation of uranium cake (as sodium diuranate).

The purity grade was evaluated through semi-quantitative EDX analysis of the precipitates. It is noteworthy that this part of the work is not supposed to be representative of the optimized recovery and separation of target metals from the ore. The main objectives consist of illustrating a complete flowsheet of treatment and showing the efficiency of the sorbents for recovering U and Th from a complex solution.

3. Results and discussion

3.1. Characterization of sorbents

3.1.1. Physical characterization

Morphology – SEM micrographs: Scanning electron microscopy shows that the grafting of either urea or thiourea changes both the size of the beads and the surface morphology (Fig. S1, see Supplementary Information). Raw silica beads are characterized by a roughly smooth surface (except some local impurities and heterogeneities) with a size ranging between 67 and 86 μm (average particle size: 82 μm). The coating of the beads with the deposition of polymerized urea or thiourea increases the size of the beads in the range 109–117 μm for UR/SiO$_2$ and 112–130 μm for TUR-SiO$_2$ (average particle size for functionalized beads: 115 μm). This is a first evidence that the functionalization of the silica material is effective (the average thickness of functionalized layer reaches 32 μm). In addition, the surface of the two sorbents becomes much more irregular, with deposition of nanoaggregates (Atta et al., 2016). The deposition of urea (or thiourea)/formaldehyde compound may block the porosity of silica particles but the irregular surfaces can contribute to partially compensate this effect (increase in external surface area). The deposition is not fully homogeneous: the aggregates are randomly distributed, in terms of both location and size.

The comparison of BET analysis of pristine silica beads, UR/SiO$_2$, and TUR/SiO$_2$ shows substantial differences in the specific surface area of the materials and their textural characteristics (Fig. S2). The coating of silica beads reduces the specific surface from 21 to 4–6 m^2 g^{-1}; this is correlated to the decrease of the pore volume from 0.098 cm^3 g^{-1} to 0.023–0.028 cm^3 g^{-1}. Consequently, the average size of the pores is increased. The coating blocks the small pore and the average pore size logically increases; in addition, the proper porosity of the polymer layer contributes to this change in the pore size. It is noteworthy that pristine silica beads have a significant hysteresis in the BET profile, contrary to functionalized materials. The N$_2$ adsorption/desorption profiles can be qualified as Type II isotherm according the IUPAC classification (Alothman, 2012); in the case of pristine silica, the hysteresis corresponds to H3 classification; which is usually associated with slit-shaped pores. For functionalized sorbents, the hysteresis loop is negligible for UR/SiO$_2$, while for TUR/SiO$_2$, the loop is more marked (but more regular and less intense than in the case of pristine silica). The functionalization blocks the smallest pores, and apparently, the blockage is more intense for thiourea.

The thermogravimetric analysis of the two sorbents shows very similar profiles (Fig. S3): the two profiles for weight loss are almost overlapped up to 500 °C; the most significant differences are observed above this temperature. Globally, the weight-loss transitions are weakly marked. The weight loss for TUR/SiO$_2$ is generally a little lower than for UR/SiO$_2$; however, at the highest temperatures, the thiourea-derivative appears to be more

stable: the stabilization plateau occurs at temperature higher than 750 °C (690 °C for UR/SiO$_2$). In addition, the final weight losses reach up to 45.5% for UR/SiO$_2$ and about 40.3% for TUR/SiO$_2$. At 800 °C, all the organic coating is degraded and the remaining material corresponds to SiO$_2$: the mineral core represents ~60% for TUR/SiO$_2$ and ~55% for UR/SiO$_2$. The similarity in the thermal properties is also highlighted by the comparison of the DrTG profiles: the main valley is detected at 271.65–271.51 °C. In addition, the DrTG is globally positive for UR/SiO$_2$ contrary to TUR/SiO$_2$. The reference material (pristine silica beads) shows a single and limited weight loss (close to 3%) assigned to water release.

3.1.2. Chemical characterization

Fig. 1 shows the FTIR spectra of pristine silica beads and functionalized materials (Table S3). Some peaks are characteristic of mineral compartment; more specifically Si-O-Si bonds are identified close to ~1108 cm^{-1}, ~800 cm^{-1}, and ~469 cm^{-1}. Other bands (overlapped to the contribution of other bonds) are reported at ~3400 cm^{-1} (OH at Si surface), and ~1630 cm^{-1} (SiO, H$_2$OSi). The grafting of urea is confirmed by the increase in the relative intensity of some peaks: for example, the additional contribution of CC stretching (overlapped with SiO, at ~800 cm^{-1}), the enlargement of the peak at ~1109 cm^{-1} (corresponding to SiOC band). The asymmetry of the peak (with a slight shoulder at ~1180 cm^{-1}) can be assigned to the contribution of another type of vibration. However, the most significant modifications are identified at 1020–1026 cm^{-1} (CN stretching), 1629 cm^{-1} (NH bending and CO/CO stretching), and 3410 cm^{-1} (NH stretching overlapped to OH stretching). For both UR/SiO$_2$ and TUR/SiO$_2$, the peaks at 714 and 665 cm^{-1} disappear after polymer coating. These peaks are generally assigned to OH out-of-plane bending vibrations (herein, at the surface of silica beads). The grafting of polymer layer is mediated by these groups; therefore, the disappearance of these signals is directly correlated to the efficient functionalization of pristine silica beads. In addition, the peak at ~1629 cm^{-1} after functionalization of the support shows a clear asymmetrical shape, which is directly attributed to the contribution of CO and NH. In the case of TUR/SiO$_2$, the presence of S-bearing groups is shown by the peak 1385 cm^{-1} (CS group), and the CS stretching vibration (at 632 cm^{-1}). The amine groups are also identified at ~1629 cm^{-1} (NH bending). These different changes confirm the effective deposition of urea- and thiourea-based (crosslinked through the reaction with formaldehyde in acidic solution) at the surface of silica beads (contribution of OH groups).

The sorption of U(VI) and Th(IV) onto functionalized silica beads is followed by some changes in the FTIR spectra (Figs. 2–3, Tables S4–S5).

For UR/SiO$_2$, the peak at ~1629 cm^{-1} decreases in intensity and enlarges (1647–1630 cm^{-1}): NH and CO groups are involved in metal binding. The peak at 1022 cm^{-1} (CN stretching) also disappears after the uptake of both U(VI) and Th(IV), because of the protonation of reactive groups and/or the interaction of nitrogen-based groups with metal ions. In the range 1550–1550 cm^{-1}, the spectra show the appearance of small peaks, probably associated with the interaction of amine groups (and or hydroxyl groups) with metal ions (Fig. S4). It is noteworthy that in the specific case of Th(IV) sorption, the intensity of the weak peak observed at ~1383 cm^{-1} is considerably increased. This peak may be partly explained by the binding of nitrate anions (through thorium nitrate uptake). In the case of Th(IV) binding onto polysulfonamide functionalized silica, the peaks associated with OH, NH and CO stretching vibrations were reduced (in intensity) and redshifted (by 10–15 cm^{-1}) (Cheira, 2020). Cheira also identified sharp peaks at 1380–1392 cm^{-1} and 1052–1042 cm^{-1} for silica and composites; these peaks were assigned to ThO vibration of thorium ions. After U(VI) binding, the asymmetry of the band at 1180–1109 cm^{-1} is enlarged. It is noteworthy that the typical signal for UO$_2^{2+}$ (at around 925 ± 10 cm^{-1}, (Hadjittofi and Pashalidis, 2014)) is not detected, being overlapped with the wide band centered on 1109 cm^{-1}. In the case of uranium biosorption using cyanobacteria, two main changes were observed in FTIR spectra (Yuan et al., 2020): these peaks appeared at 1454.1 cm^{-1} and 916.0 cm^{-1}. Actually, these peaks overlap here with existing signals coming from CN stretching (amide) and OH bending (SiOSi and SiOC groups) vibrations. The increased intensity and broadness after uranyl binding means that these groups contribute to metal binding. This is consistent with the strong interaction between uranyl and oxygen-bearing functional groups (Zhang et al., 2014; Zhao et al., 2019).

After five cycles of sorption and desorption, the spectra are only partially restored; meaning that the functional groups are irreversibly modified by the binding of the sorbent and/or the successive treatment (with different levels of acidity). In the case of TUR/SiO$_2$, the most significant changes are reported again in the region 1800–1300 cm^{-1}: the 1630 cm^{-1} asymmetric sharp peak is replaced by a broad band (with increased contributions of side shoulders), similarly to uranyl sorption by UR/SiO$_2$. This result confirms that metal binding occurs through amine groups with possible contribution of OH groups. After metal desorption, this peak is closely restored to its initial shape. The peak (assigned to CS stretching) at 1452 cm^{-1} disappears after metal binding (and this peak is not totally restored after metal desorption): thiocarbonyl groups are also involved in metal binding. This effect of metal binding on sulfur-based groups is also demonstrated by the appearance of a new peak in the region 2558–2563 cm^{-1}; the relative
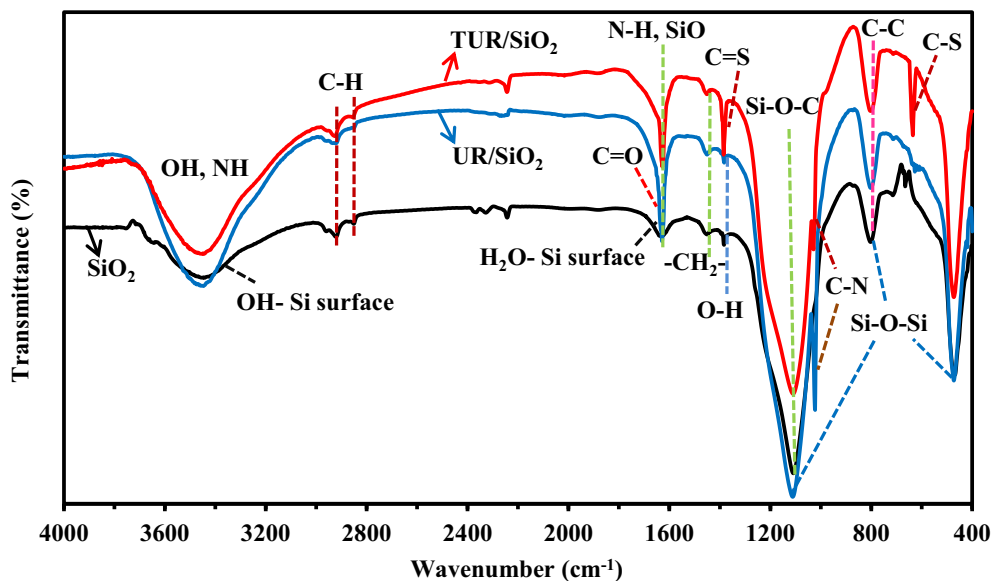

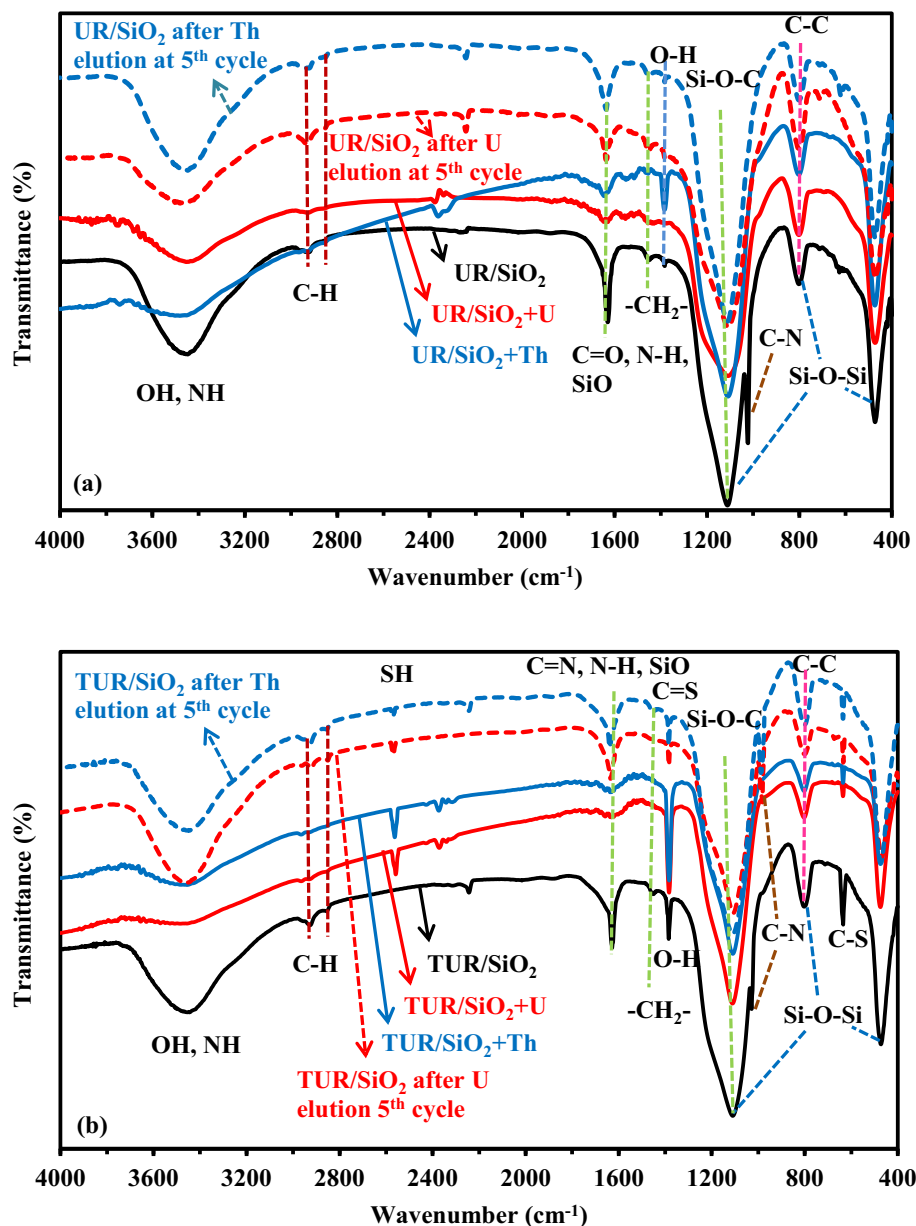Fig. 1. FTIR spectra of SiO$_2$, UR/SiO$_2$, and TUR/SiO$_2$ materials.

Fig. 2. FTIR spectra of UR/SiO$_2$ (a) and TUR/SiO$_2$ (b) materials before and after metal sorption (and after elution at the fifth recycling) (sorbents were collected from sorption isotherm experiments performed at pH$_0$ 4, with sorbent dose, SD: 0.666 g L^{-1}; $C_0 \sim 2.1$ mmol L^{-1}).

intensity of this peak apparently decreases with metal desorption. The large band (poorly resolved) at 3445 cm^{-1}, which corresponds to overlapped contributions of OH and NH stretching vibrations, is shifted toward higher wavenumbers after sorption of both U(VI) and Th(IV) and for both UR/SiO$_2$ and TUR/SiO$_2$. This is another evidence of the cross-contributions of NH and OH for metal binding. These conclusions (completed by the interpretation of pH effect, see below) allow suggesting different modes of interactions of the two sorbents with U(VI) and Th(IV) (Scheme 2).

3.1.2.1. Elemental analysis. The elemental analysis of the two sorbents shows very similar nitrogen content (i.e., ~8.1%, w/w, or ~5.78 mmol N g^{-1}) (Table S6). In the case of TUR/SiO$_2$, S-content reaches ~4.8%, w/w (i.e., 1.51 mmol S g^{-1}). The molar ratio S/N is close to 0.26, while the expected ratio (based on the structure of thiourea and sorbent, Scheme 1) would be close to 0.5. This means that the actual mode of synthesis does not allow maintaining the stability of thiourea: sulfur group is probably

cleaved by reaction of thione with amines from adjacent chains. Actually, only 50% of S-moieties from thiourea are retained on the sorbent.

On the other hand, the total weight fraction of these elements (C, H, O, N, and S) represent around 73%, meaning that Si represent about 27% (in weight). Therefore, SiO$_2$ represents about 57.8%; this is consistent with the TGA analysis, which showed that the mineral fraction represent about 60% for TUR/SiO$_2$ and 55% for UR/SiO$_2$ (see Section 3.1.1)

3.1.2.2. pH$_{PZC}$. The application of the pH-drift method allows determining the total surface charge of the sorbents in function of the pH of the solution, and deducing their pH$_{PZC}$ values (Fig. S5) (Lopez-Ramon et al., 1999): 5.79 ± 0.06 and 5.22 ± 0.04 for UR/SiO$_2$ and TUR/SiO$_2$, respectively. The ionic strength of the background solution (NaCl) hardly influences the determination of pH$_{PZC}$ values. The pK$_a$ values of urea and thiourea compounds are 26.9 and 21.1, respectively (Gómez et al., 2005): thiourea is more acidic than urea, consistently with the shift in their pH$_{PZC}$ values on composite materials. UR/SiO$_2$ is positively charged in a wider range of
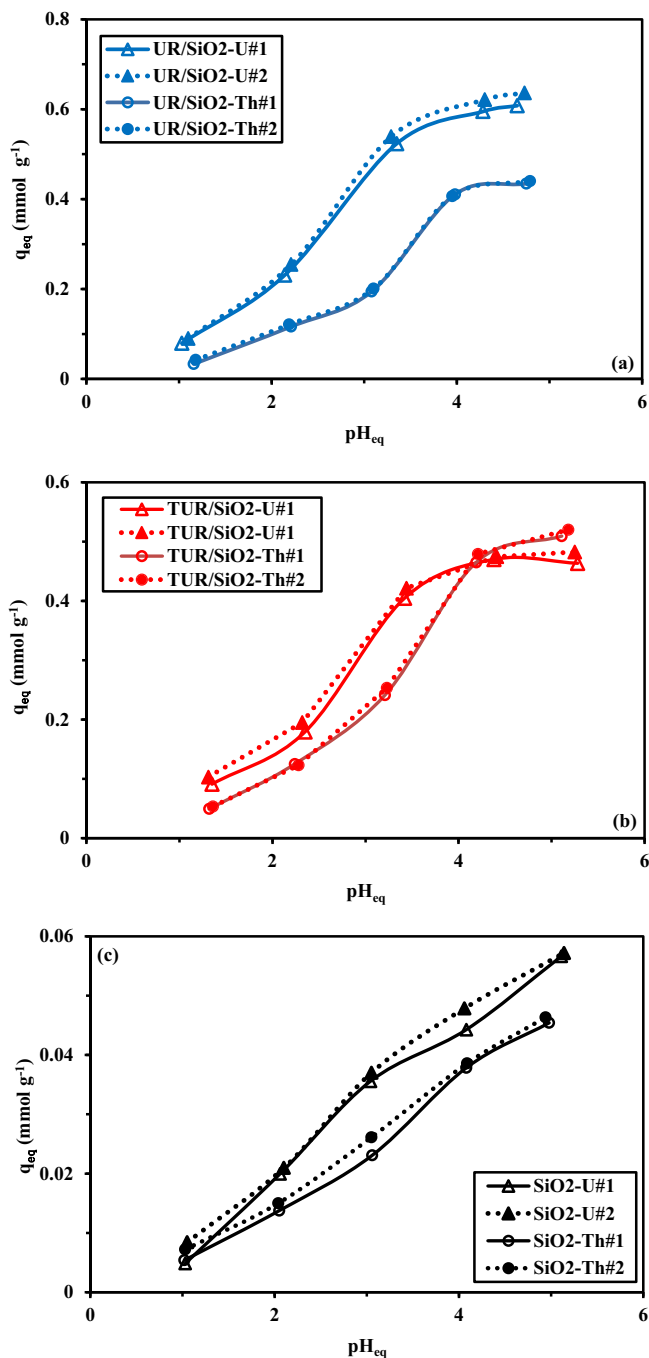
Fig. 3. Effect of pH on U(VI) and Th(IV) sorption using UR/SiO$_2$ (a), TUR/SiO$_2$ (b) and pristine SiO$_2$ (c) sorbents at T: 22 $\pm$ 1 °C (C_0: 0.225 mmol L^{-1}; SD: 1 g L^{-1}; agitation time: 48 h; v: 210 rpm; duplicate experiments: Series #1 and #2).

of metal cations; this repulsion decreases as pH increases and tends to be negligible at pH$_{PZC}$ values (i.e., 5.81 and 5.27, respectively). It is noteworthy that the silanol groups at silica surface are acidic; they contribute to modulate the acid-base properties of the composite. However, the coating of the beads with the polymer layers partially masks this effect.
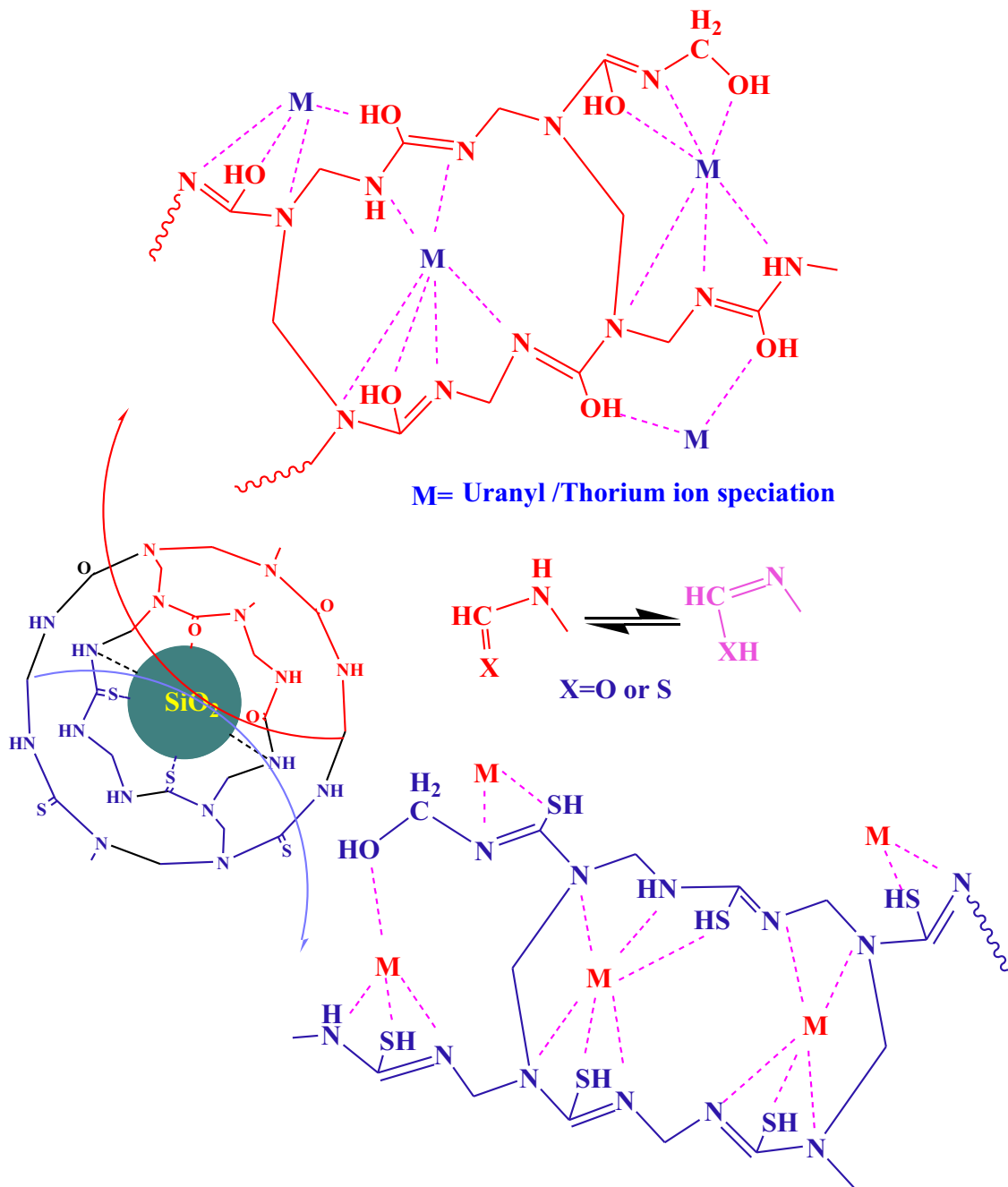
3.2. Sorption properties

3.2.1. Effect of pH

The pH strongly influences the sorption of both U(VI) and Th(IV) by UR/SiO$_2$ and TUR/SiO$_2$ (Figs. 3–4) at two temperatures: T = 22 $\pm$ 1 °C and T = 50 $\pm$ 1 °C. The trends are roughly the same for low and high temperatures. Fig. S6 shows the sorption properties of pristine silica beads under the same experimental conditions: the sorption capacities are drastically reduced below 0.06 mmol U g^{-1} and below 0.05 mmol Th g^{-1}. Taking into account the fraction of silica into the composite (between 55 and 60%); this means that the contribution of silica support represents less than 0.03 mmol g^{-1} (in other words, negligible; less than 5% of the total sorption reported for functionalized silica beads). This simple comparison clearly demonstrates the beneficial effect of the functionalization of the support on the intrinsic properties of the sorbent for capturing uranium and thorium. This means also that silica mainly acts as a support for functionalized polymer layers.

The duplication of experimental series confirms the reproducibility of the sorption properties. In acidic solutions (i.e., pH$_{eq}$ 1–1.3), the sorption capacities remain below 0.1 mmol g^{-1}. The sorbents are strongly protonated and may repulse metal cations. Free uranyl cation (i.e., UO$_2^{2+}$) is present and largely predominant at pH 4; hydrolyzed cationic polynuclear species may coexist above pH 4 (Fig. S7a). The high density of positively charged reactive groups strongly repulses free UO$_2^{2+}$ species, while the increase of the pH enhances metal sorption. Free Th(IV) predominates at pH below 3, while hydrolyzed cationic species appears at higher pH values; precipitation may occur at pH higher than 4–4.5 (Chen and Wang, 2007; Chen et al., 2007; Esen Erden and Donat, 2017; Hu et al., 2017; Sheng et al., 2008) (Fig. S7b). Thorium globally follows the same trends as U(VI). The distribution of metal species is very debated (Moulin et al., 2001); however, it is commonly accepted that thorium is less soluble than uranyl, while its hydrolyzed species, such as Th(OH)$_3^+$, Th(OH)$_2^{2+}$, Th(OH)$_3^+$ and Th(OH)$_4$, are formed at lower pH values (Esen Erden and Donat, 2017). The highest increases in sorption capacities are reported for pH$_{eq}$ varying between 2.3 and 4, while at higher pH, the sorption tends to stabilize. The appearance of polynuclear hydrolyzed U species (and hydrolyzed Th species) reveals unfavorable for the binding of metal ions on these amine-bearing sorbents. The presence of thiocarbonyl groups brings alternative groups (to carbonyl groups); however, the sorption properties are slightly decreased. This may be explained by the smaller charge of thiocarbonyl cation compared with carbonyl group (consistently with the difference in electronegativity between O and S (Wiberg and Wang, 2011)). U(VI) and Th(IV) are classified as hard acids according the hard and soft acid base principle (Pearson, 1966); they are expected to have higher reactivity with hard bases (i.e., O-bearing ligands are more reactive than S-bearing ligands). Other reactive groups (i.e., N-bearing) being the same (same content), the difference in sorption capacities between UR/SiO$_2$ and TUR/SiO$_2$ is thus directly related to the highest reactivity of carbonyl groups compared with thiocarbonyl groups.

The profiles for U(VI) and Th(IV) are very similar for TUR/SiO$_2$: the sorption of U(VI) is slightly greater, except at pH$_{eq}$ close to 5 (where thorium may begin to form colloidal Th(OH)$_4$ species). For UR/SiO$_2$, the differences are more marked: sorption capacities are about 0.1–0.3 mmol higher for U(VI) than those observed for Th(IV). The highest difference is observed at pH$_{eq}$ 3, making possible preferential concentrative effect of U(VI) over Th(IV) (this effect is less detectable while considering the treatment of ore leachates, see below), while using UR/SiO$_2$, a weaker effect is expected for TUR/SiO$_2$. The difference in sorption capacities may be correlated with the difference in the electronegativity of U(VI) (i.e., 1.7, according Pauling's scale) and Th(IV) (i.e., 1.3) (RSC, 2020), while their hydrated radius are

pH values, and the deprotonation of amine groups on TUR/SiO$_2$ occurs at a lower pH value. The relative properties of carbonyl and thiocarbonyl correlate with the highest electronegativity of O compared with N groups (Wiberg and Wang, 2011). This is consistent with the intrinsic properties of urea and thiourea precursors, despite the probable degradation of thiourea during the synthesis procedure (see discussion of elemental analysis). In the acidic pH region, the sorbents will be positively charged. The density of charge is correlated to the amplitude of pH change: UR/SiO$_2$ is significantly more charged than TUR/SiO$_2$. Largest pH variations occur at pH$_0$: ~4: equilibrium pH increases by up to 0.85 for UR/SiO$_2$ and 0.53 for TUR/SiO$_2$. The protonation of reactive groups contributes to the repulsion

Scheme 2. Tentative mechanisms for the sorption of U(VI) and Th(IV) using UR/SiO$_2$ and TUR/SiO$_2$.

comparable (1.08 Å for U(VI) and 1.11 Å for Th(IV)) (Persson, 2010) (Table S7).

The sorption process is accompanied by a moderate increase of the pH that does not exceed 0.3 pH unit (i.e., much lower than the pH variations observed in the determination of pH$_{PZC}$ values) (Fig. S8 at T: 22 °C, and Fig. S9 at T: 50 °C). Fig. S6b shows that the sorption process does not affect the equilibrium pH value in the case of pristine silica beads, at least less than in the case of functionalized materials, where the reactive groups bring their proper acid-base interactions. In addition, the higher binding of metal ions induces larger proton releases for functionalized materials.

The distribution ratio (D) is defined as the ratio q$_{eq}$/C$_{eq}$. Plotting log$_{10}$ D *vs.* pH$_{eq}$ is frequently used for determining the molar ratio between proton release and metal binding (as the slope of the curve). Fig. S10 compares the log$_{10}$ plots of the distribution ratio *vs.* pH$_{eq}$ for the two sorbents at T: 22 °C and T: 50 °C. Table S8 reports the values for the different systems (sorbent/

metal) at two temperatures (i.e., 22 and 50 °C). In the case of UR/SiO$_2$, the molar ratio is close to 0.5 (~0.575) for U(VI): two protons may be released per sorbed uranyl ion. It is noteworthy that the temperature hardly affects the slope for this sorbent. Temperature has a more marked effect on TUR/SiO$_2$. Indeed, the slope decreases with increasing the temperature (from 0.32 to 0.24 and from 0.425 to 0.37, for U(VI) and Th(IV), respectively); the molar ratio would be closer to 0.33 (three protons released per bound metal). Similar trend is identified for Th(IV) sorption onto TUR/SiO$_2$ (from 0.43 to 0.36). It is noteworthy that for UR/SiO$_2$ the stoichiometric ratio is higher for U(VI) than for Th(IV), whatever the temperature. On the opposite hand, for TUR/SiO$_2$ the stoichiometric ratio is greater for Th(IV) than for U(VI). The differences in the functional groups on the sorbents and the differences in the chemistry of U(VI) and Th(IV) significantly affect the molar ratios and the sensitivity to pH. It is noteworthy that increasing the temperature from 22 ± 1 °C to 50 ± 1 °C weakly
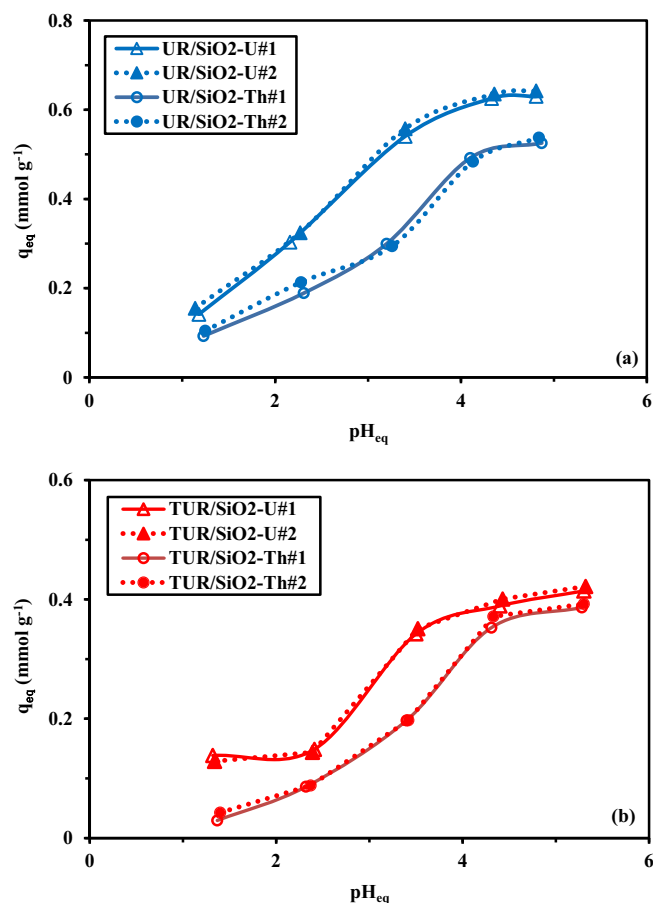
Fig. 4. Effect of pH on U(VI) and Th(IV) sorption using UR/SiO₂ (a) and TUR/SiO₂ (b) sorbents at T: 50 ± 1 °C (C_0: 0.225 mmol L^{-1}; SD: 1 g L^{-1}; agitation time: 48 h; v: 210 rpm; duplicate experiments: Series #1 and #2).

changes the sorption performance. Regardless of the metal, in the case of UR/SiO₂, the sorption is slightly increased by increasing the temperature: the sorption is slightly endothermic. The reciprocal trend is observed for TUR/SiO₂; the sorption appears to be slightly exothermic, with a little decrease in sorption properties at higher temperature. It is noticeable that the variations are relatively limited for a temperature gap as large as 30 °C. This figure also confirms that for Th(IV) the two sorbents have close behaviors, while for U(VI) the superiority of UR/SiO₂ is demonstrated, especially with increasing the pH.

Fig. S11 shows the semi-quantitative EDX analysis of the surface of the sorbents after U(VI) and Th(IV) sorption. The metals are efficiently bound with weight fractions in the range 3.2–4.2% (i.e., 1.9–3.1%, atomic concentrations). EDX analyses are semi-quantitative and must be considered as simply indicative: apparently UR/SiO₂ binds more U(VI) than Th(IV) contrary to TUR/SiO₂, where Th(IV) sorption is slightly higher than for U(VI) (probably due to the contribution of the binding or precipitation of colloidal hydrolyzed species).

Based on the FTIR analysis of sorbents, sorbent titration, and the interpretation of pH effect, it is possible supporting Scheme 2 with the following arguments:

a. The pH$_{PZC}$ (close to pH 5) indicates that the sorbent is partially protonated during sorption experiments (at pH 4). Therefore, electron pairs are available for chelation (from thiols, amines and hydroxyl groups), as well as ion exchange properties due to protons that can be exchanged with cationic species of metal ions.

b. FTIR analysis showed decreasing intensities of the peaks assigned to the reactive groups involved in sorption (such as OH and SH signals). The shifts of other peaks (such as those associated with CO and CS), the

disappearance of CS (which is involved in tautomerization rearrangement) can be correlated with the binding of metal ions.

c. The log$_{10}$ plots of the distribution ratio *vs.* pH$_{eq}$, gives also complementary information. In the case of UR/SiO₂, the molar ratio is close to 0.5 (≈ 0.575) for U(VI): this means that two protons may be released per sorbed uranyl ion (which is mainly found as UO$_2^{2+}$). A different trend is identified for Th(IV) sorption onto TUR/SiO₂ (from 0.43 to 0.36), which means three protons were exchanged by bound metal. However, this interpretation is made complex by the co-existence of different metal species bearing different global charge.

3.2.2. Sorption kinetics

Under selected experimental conditions (i.e., sorbent dose, SD: 0.667 g L^{-1}; C_0: 0.44 mmol L^{-1}; v: 210 rpm), the equilibrium is reached within 60–120 min, with residual relative concentrations in the range ~0.15–0.3 (Fig. 5). These kinetic profiles are relatively fast; however, taking into the average size of the functionalized silica beads (in the range 110–130 μm), this order of magnitude for equilibrium time indicates that the contribution of resistance to intraparticle diffusion to the overall control of uptake kinetics cannot be neglected. A substantial difference can be observed in the kinetic behavior of UR/SiO₂ and TUR/SiO₂: The kinetic profiles for U(VI) and Th(IV) are superposed in the case of urea-functionalized silica beads, while for the thiourea derivative, the sorption of U(VI) is both slightly faster and more efficient than that of Th(IV). A steeper initial slope is observed for duplicated curves of U(VI) binding onto UR/SiO₂ (compared with Th(IV)), and the equilibrium sorption capacities reach ~0.45 mmol Th g^{-1} and up to ~0.55 mmol U g^{-1}.

Sorption kinetics may be controlled by different mechanisms such as resistance to bulk diffusion, film diffusion or intraparticle diffusion, in addition to the proper reaction rates (approached with the pseudo-first or pseudo-second order rate equations, PFORE and PSORE, respectively, Table S1a). Preliminary tests showed that maintaining the agitation speed above 200 rpm avoids sorbent sedimentation and minimizes the resistance to bulk and film diffusion (initial slope of the concentration decay curve). The preliminary comment (see above) stated that the resistance to intraparticle diffusion plays a non-negligible role; the Crank equation (RIDE, Table S1a) was used for modeling the kinetic profile and approaching the determination of the effective intraparticle diffusion coefficient (D_e, m^2 min^{-1}). Table S9 summarizes the parameters of the different models (and the comparison of statistical criteria: determination coefficient, R^2 and Akaike information criteria, AIC). The PFORE systematically fits better the experimental profiles than the PSORE and the RIDE. In Fig. 5, the lines show the simulation of kinetic profiles with the PFORE; the PSORE and the RIDE modeled curves are appearing in Figs. S12–S13. The calculated q_{eq} values ($q_{eq,1}$) are slightly higher (by 4–9%) than the experimental values. The values of apparent rate coefficients for PFORE (k_1) confirm the shape of the kinetic curves observed in Fig. 5. The rate coefficients are a little higher for U(VI) than for Th(IV), whatever the sorbent. On the other hand, UR/SiO₂ shows little higher apparent rate coefficients than TUR/SiO₂ for both U(VI) and Th(IV). It is noteworthy that these differences are relatively weak; indeed, the k_1 parameter globally varies in the range 0.036–0.050 min^{-1}.

In the literature, the temptation is frequent to correlate the fitting of experimental profiles with given models to physical *vs.* chemical sorption. Hubbe's group recently analyzed the literature on systems modeled with the PSORE (Hubbe et al., 2019). They observed that frequently, the experimental conditions are not perfectly designed to make possible the appropriate fitting of experimental profiles with physical soundness. More specifically, they concluded that in many cases, the fitting of the kinetic profiles (with inappropriate experimental design) may be associated with the kinetic control through resistance to intraparticle diffusion. Therefore, the assignment of the type of sorption mechanism simply based on mathematical models may be debatable. Herein, the residual metal concentration being far from the initial metal concentration, the required assumptions for application of PSORE are not fulfilled. The determination of apparent rate coefficients may be globally considered as a first approximation and a
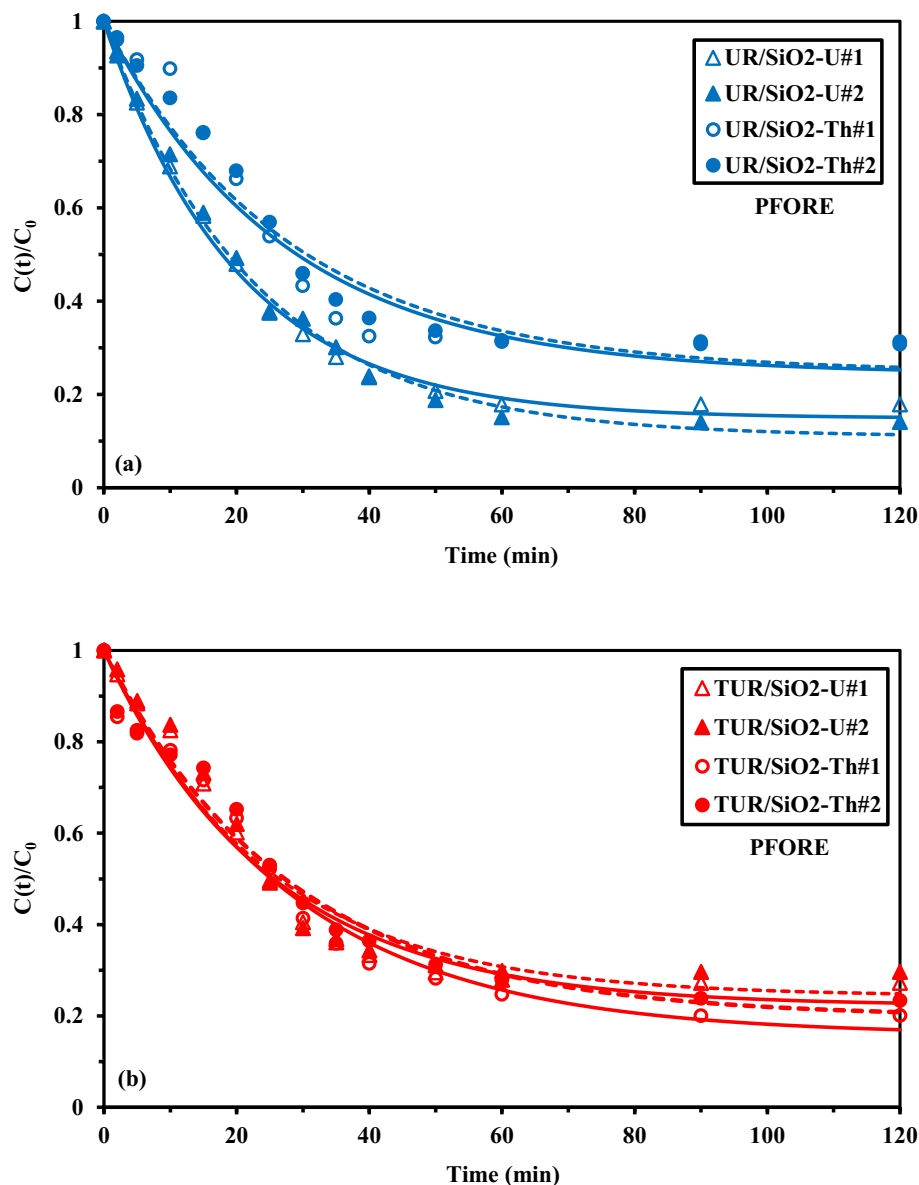
Fig. 5. U(VI) and Th(IV) uptake kinetics using UR/SiO$_2$ (a) and TUR/SiO$_2$ (b) sorbents – modeling with the PFORE (*SD*: 0.667 g L^{-1}; C_0: 0.44 ± 0.1 mmol L^{-1}; pH$_0$: 4; *v*: 210 rpm; *T*: 22 ± 1 °C).

simple tool for comparing the systems (without assigning these profiles to sorption mechanisms).

The intraparticle diffusion coefficients are in the range 0.9–83 × 10^{-11} m^2 min^{-1}, this is several orders of magnitude lower than the molecular diffusivity of metal ions in water (for example 2.56 × 10^{-8} m^2 min^{-1} for U (VI), (Marcus, 1997)). This is a confirmation that the resistance to intraparticle diffusion contributes to the control of uptake kinetics. In the case of TBP-impregnated sorbent, Abdel Raouf and El-Kamash found diffusivity coefficients close to 1.02 × 10^{-10} m^2 min^{-1} for U(VI) and 1.14 × 10^{-10} m^2 min^{-1} for Th(IV) (Abdel Raouf and El-Kamash, 2006). It is noteworthy that in the case of TUR/SiO$_2$ the diffusivity coefficients are comparable for U(VI) and Th(IV) (0.93–1.53 × 10^{-11} m^2 min^{-1}) and of the same order of magnitude as Th(IV) for UR/SiO$_2$; contrary to U(VI) diffusivity for urea-functionalized silica beads (where the diffusivity is about 50 times greater). Despite the variation in the value of the apparent diffusivity between the duplicated experiments, such a big difference is significant but difficult to explain.

Fig. S14 compares the kinetic profiles for the sorption of U(VI) and Th (IV) from bi-component equimolar solutions on both UR/SiO$_2$ and TUR/

SiO$_2$. In the case of UR/SiO$_2$, the affinity for U(VI) is higher than that for Th(IV), consistently with previous trends from mono-component solutions. The equilibrium concentration and the equilibrium time are lower and the initial slope is steeper for uranyl compared with Th(IV). On the other hand, for TUR/SiO$_2$ the initial slopes are comparable for the two metal ions, while the equilibrium time is shorter for U(VI) and the equilibrium concentration is higher for uranyl. TUR/SiO$_2$ is more favorable for thorium recovery than uranium in binary solutions. This is globally consistent with the trends reported below in the study of selectivity. It is noteworthy that in the case of mono-component solutions, the profiles were superposed for U(VI) and Th(IV); in the case of binary solutions, the slight preference of thiourea-functionalized silica beads for Th(IV) over U(VI) shifts the equilibrium favorably to thorium.

3.2.3. Sorption isotherms

The sorption isotherms represent the distribution of sorption capacities – or concentration of the sorbate on the sorbent – as a function of residual metal concentration; q_{eq} = f(C_{eq}). This is a useful tool for qualifying the sorption properties of the material through two criteria: the maximum

sorption capacity (at saturation of the monolayer), and the initial slope of the curve (which is indicative of the affinity of the sorbent for the target metal). Fig. 6 compares the sorption isotherms for U(VI) and Th(IV) using both UR/SiO$_2$ and TUR/SiO$_2$ at pH 4. The urea-functionalized silica beads are slightly more efficient for U(VI) sorption than TUR/SiO$_2$ uptake (both in terms of affinity and maximum sorption capacity). The steeper initial slope (correlated with the affinity coefficient) for U(VI) confirms the higher efficiency of UR/SiO$_2$ compared with that of TUR/SiO$_2$. An opposite trend is observed for Th(IV): highest sorption capacities and affinities are observed for TUR/SiO$_2$ sorbent. The two sorbents have comparable contents of amine groups; the main difference consists of the substitution of carbonyl with thiocarbonyl groups. The relative changes in affinity and sorption capacities for UR/SiO$_2$ and TUR/SiO$_2$ may be explained by the fact that: (a) S-based ligands are more reactive with hard acids than O-based ligands, and (b) the Pauling electronegativity of U(VI) is higher than that of Th(IV).

The sorption isotherms can be fitted using conventional models (Langmuir, Freundlich, and Sips equations, for example; Table S1b). Fig. 6 clearly shows a saturation plateau reached for residual concentrations close to 1.5 mmol L^{-1}. The Freundlich equation being a power-type equation is not appropriate for describing this kind of isotherm shape. On the opposite

hand, the Langmuir model supposes that the sorption occurs by monolayer adsorption, without interactions between sorbed molecules and with homogeneous sorption energies (including homogeneous distribution of sorption sites at the surface of the sorbent). The Sips equation combines Langmuir and Freundlich terms. This equation offers a third-adjustable parameter that usually improves the mathematical fit of experimental profiles (at the expense of a loss in physical soundness). Table S10 compares the maximum experimental sorption capacities to the maximum sorption capacities calculated from Langmuir and Sips equations; the other parameters are reported together with statistical criteria (R^2 and AIC) for efficient comparison of mathematical fits. Duplicate isotherms confirm the reproducibility of sorption performances and the robustness of mathematical fits: the Langmuir and the Sips equations give relatively good simulations of experimental profiles. In Fig. 6, the lines represent the Langmuir fits of experimental curves (the fits with the Sips equation are reported in Fig. S15). The maximum sorption capacities are comparable for the different systems: between 0.89 and 1.16 mmol g^{-1} for $q_{m,exp}$ and between 1.01 and 1.18 mmol g^{-1} for $q_{m,L}$. The affinity coefficients are more favorable for U(VI) and UR/SiO$_2$, while TUR/SiO$_2$ shows a little greater affinity for Th(IV) than for U(VI). This conclusion is consistent with previous discussions on the relative preference of UR/SiO$_2$ for U(VI) and TUR/SiO$_2$ for Th(IV),
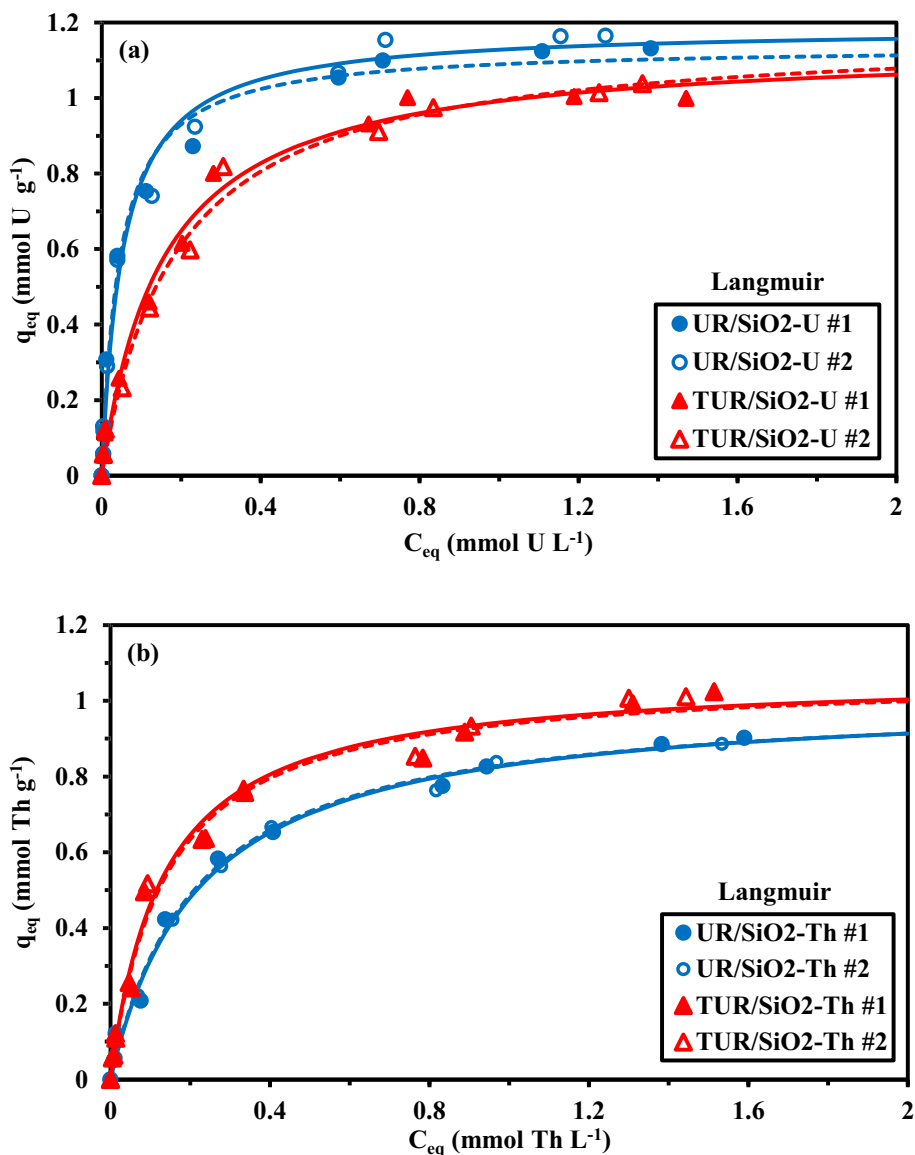

Fig. 6. U(VI) (a) and Th(IV) (b) sorption isotherms at pH$_0$: 4 using UR/SiO$_2$ and TUR/SiO$_2$ – Modeling with Langmuir equation (*SD*: 0.666 g L^{-1}; time: 48 h; C_0: 0.04–2.14 mmol U L^{-1} or 0.04–2.20 mmol Th L^{-1}).

as derived from the study of pH effect. Alternative models (including Temkin and Dubinin-Radushkevich equations) have been used for modeling experimental profiles (see Figs. S16–17).

Complementary investigations were performed at T: 30 °C, 40 °C and 50 °C, for evaluating the impact of temperature on sorption performance and calculating the thermodynamic parameters. The results are summarized in Figs. S18–21 (lines representing the Langmuir fits). Tables S11–14 report the parameters of the different models for the sorption of U(VI) and Th(IV) using UR/SiO$_2$ and TUR/SiO$_2$ at different temperatures. The study of the temperature effect on the sorption of U(VI) and Th(IV) using UR/SiO$_2$ and TUR/SiO$_2$ shows strong differences for the two sorbents (Figs. S16–17). These differences are marked in both terms of maximum sorption capacity (saturation plateau) and initial slope analysis. First of all, for both U(VI) and Th(IV), the sorption onto UR/SiO$_2$ is enhanced with temperature, while that onto TUR/SiO$_2$ decreases: metal sorption is endothermic for UR/SiO$_2$, while for TUR/SiO$_2$ the reaction is exothermic. The affinity coefficients (b$_L$) were used in van't Hoff equation for calculating the thermodynamic parameters: ΔH° and ΔG°, the enthalpy and Gibbs free energy changes (kJ mol^{-1}) and ΔS°, the entropy change (J mol^{-1} K^{-1}) (Tran et al., 2021).

$$\Delta G^{\circ} = -RT\ln K_{eq}^{0} = -RT\ln b_{L}^{*} = -RT \ \ln\left[b_{L} \times \frac{C_{adsorbate}^{0}}{\gamma_{adsorbate}}\right] \tag{1}$$

$$\Delta G^{\circ} = \Delta H^{\circ} - T\Delta S^{\circ} \tag{2}$$

where C°$_{adsorbate}$ is the unitary standard concentration of the adsorbate (≈ 1 mmol L^{-1}) and γ$_{adsorbate}$ is the activity coefficient of the adsorbate (usually considered close to the unity in the case of diluted solutions).

Fig. S22 shows the plots of ln b$_L$* vs. the reciprocal of absolute temperature. The analysis of slope and ordinate intercept allows determining the thermodynamic parameters, which are summarized in Table S15. As expected, for UR/SiO$_2$, the positive values for enthalpy change confirm the endothermic sorption of both U(VI) and Th(IV). It is noteworthy that the enthalpy change is significantly greater for Th(IV) compared with U(VI) sorption. On the other hand, for TUR/SiO$_2$, similar negative values of the enthalpy change confirm the exothermic behavior of sorption (similar values for U(VI) and Th(IV)). The adverse effect of temperature is usually associated to physical sorption, while the enhancement of sorption with temperature (at least in a first step) is frequently associated with chemisorption (which needs higher activation energy).

The values of entropy changes are also opposite for UR/SiO$_2$ (positive, and greater for Th(IV) than for U(VI)) and TUR/SiO$_2$ (negative, and comparable for the two metals: $-39.8/-42.2$ J mol^{-1} k^{-1}). With UR/SiO$_2$, metal sorption is followed by an increase in the randomness of the system contrary to TUR/SiO$_2$, which shows a more conventional evolution of entropy change (i.e., negative values).

For the different systems, the values of Gibbs free energy are negative in a very narrow range (i.e., between -20 and -30 kJ mol^{-1}); the sorption process is spontaneous. As expected, the spontaneity is slightly greater for UR/SiO$_2$ than for TUR/SiO$_2$ and varying under reverse trends for the two sorbents with temperature increase (favorable for UR/SiO$_2$ and less favorable for TUR/SiO$_2$).

These different results confirm the strong difference in the mechanisms involved in metal binding for silica beads functionalized with either urea or thiourea: predominance of chemical vs. physical sorption, respectively.

Table S16 reports the sorption performances of alternative sorbents appearing in recent publications. Though UR/SiO$_2$ and TUR/SiO$_2$ are not appearing among outstanding sorbents such as pycolylamine (Liu et al., 2017) or functionalized MCM-41 silica (Bayramoglu and Arica, 2016) for U(VI), and magnetic/rosin amidoxime (Atta and Akl, 2015) or carbon nanofiber/polymer composite (Tuzen et al., 2020) for Th(IV), the sorbents have interesting combined performances (relatively fast, good sorption levels and affinity), compared to most of reported sorbents. The actual fraction of polymer in the composite sorbent does not exceed 40–50%; this means that converting the sorption capacities to the effective amount of reactive

coatings confirms the high efficiency of UR- and TUR-layers for binding both U(VI) and Th(IV). Indeed, as shown in Fig. S6a, the sorption of pristine SiO$_2$ remains negligible (below 5% of the sorption capacities reported with functionalized SiO$_2$, under selected experimental conditions).

3.2.4. Selectivity – sorption from multi-metal solutions

The complexity of real effluents may affect the sorption performance of target elements. Investigating the selectivity is thus a requisite for evaluating the effective potential of new sorbents. The sorption of U(VI) and Th(IV) from multicomponent equimolar (1 mmol L^{-1}) solutions at different pH values for both UR/SiO$_2$ and TUR/SiO$_2$ is shown in Fig. 7, as the selectivity coefficient for U(VI) and Th(IV) against other metal ions present in the solution. The selectivity coefficient (for example, $SC_{U/Metal}$) is defined as the ratio of distribution coefficients:

$$SC_{U/Metal} = \frac{D_U}{D_{Metal}} = \frac{q_{eq,U} \times C_{eq,Metal}}{C_{eq,U} \times q_{eq,Metal}} \tag{3}$$

Competitor metal ions (and metalloid) are selected among those usually present in the leachates of Egyptian ores: Ca(II), Mg(II), Si(IV), and Al(III) (for aluminosilicate minerals), Fe(III) and Zn(II) (for usual heavy metals). The figure shows that, in most cases, the selectivity for U(VI) and Th(IV) increases with equilibrium pH. Some local dispersions in the trends may be observed for Mg(II), Fe(III), Al(III), and Zn(II) at intermediary pH (i.e., 3.3–3.5), especially for UR/SiO$_2$. The two sorbents show marked preference for U(VI) and Th(IV) against the other metals. In addition, UR/SiO$_2$ is slightly more selective than TUR/SiO$_2$. This may be explained by the presence of thiocarbonyl group, where the S-bearing ligand is classified as a softer ligand (compared with O-bearing ligand); consequently, the functional groups may also interact with a wider range of other heavy metal ions. This contributes to the decrease in the selectivity. Table S17 reports the physico-chemical properties of selected metal ions (Lewis acid character, solution-phase electronegativity, Pauling electronegativity, enthalpy of hydration, ionic radius and softness). Regarding the selectivity between U(VI) and Th(IV), the coefficients are much lower than for the other competitor metals. In the case of UR/SiO$_2$, whatever the pH, the sorbent has a weak preference for U(VI) against Th(IV): the $SC_{U/Th}$ is systematically greater than 1 (decreasing from 2.8 to 1.5 with increasing the pH). In the case of TUR/SiO$_2$, the preference is controlled by the pH: at low pH (i.e., pH 1.43), the sorbent preferentially binds U(VI) ($SC_{U/Th}$ is close to 1.43); on the opposite hand, when the pH increases to 4.98, the sorbent marks a weak preference for Th(IV) ($SC_{Th/U} \sim 1.48$). These weak SC values mean that the two sorbents will not be effective for the separation of these two actinides. As a general conclusion, working at pH close to 5 allows separating U(VI) and Th(IV) from heavy metals and UR/SiO$_2$ is slightly more efficient for the selective recovery of uranium and thorium.

Fig. S23 provides another perspective on selective separation: the distribution ratios (D, in log$_{10}$ units) are plotted against the equilibrium pH for the different systems. The curves for U(VI) and Th(IV) are clearly out of the trends followed by the other competitor ions, and the shift (also marked by the relevant slopes) is accentuated when the pH increases to 4–5. The separation efficiency (associated with high D values) increases with the pH, and the relative positions of the linearized curves confirm that UR/SiO$_2$ has a preference for U(VI) against Th(IV), contrary to TUR/SiO$_2$ (where the curves are almost overlapped).

Fig. S24 shows the semi-quantitative analysis of the sorbents after being exposed to multi-metal solutions at pH 5. Though the sorbents bear higher contents of U(VI) and Th(IV), the sorbents also accumulate substantial amounts of Fe > Ca, Zn, Al, Mg.

3.2.5. Metal desorption and sorbent recycling

Metal desorption and sorbent recycling are also important criteria in the development of new sorbents. There are three main strategies for desorbing accumulated metal ions from loaded supports: (a) changing the pH (for reversing the equilibrium for systems where the pH strongly influences metal binding), (b) using a complexing agent (for displacing the equilibrium
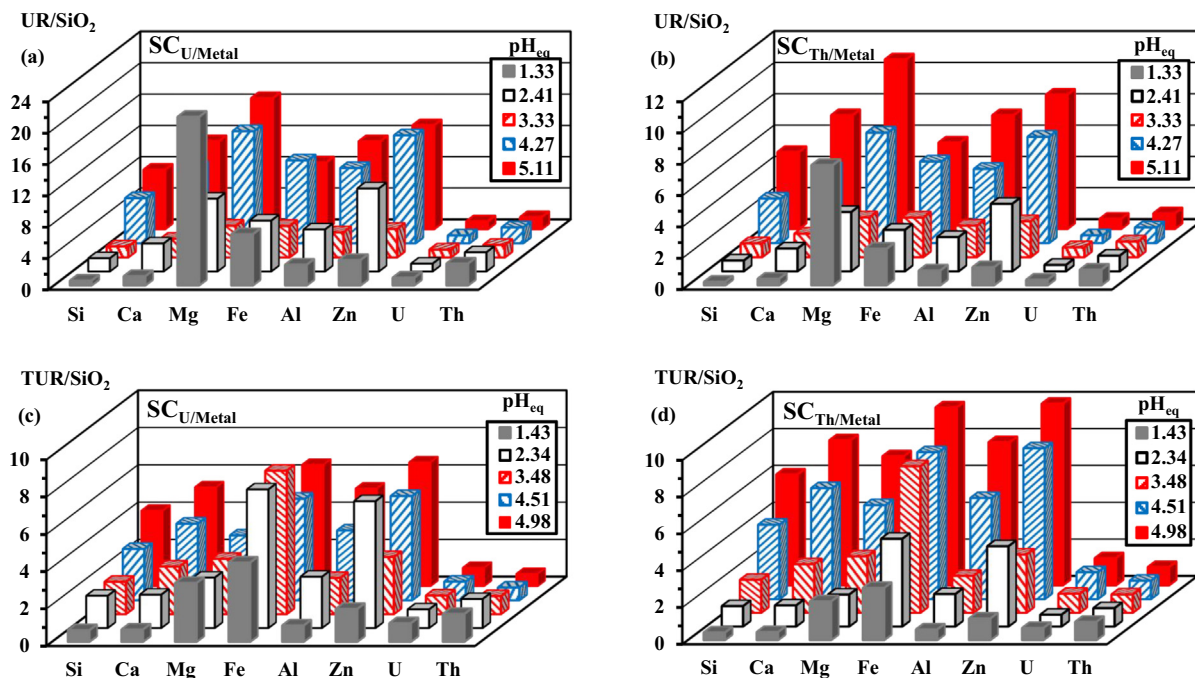
Fig. 7. Selectivity tests for the sorption of U(VI) and Th(IV) from multi-component equimolar solutions at different pH values for UR/SiO$_2$ (a: $SC_{U/Metal}$ and b: $SC_{Th/Metal}$) and TUR/SiO$_2$ (c: $SC_{U/Metal}$ and d: $SC_{Th/Metal}$) (SD: 5 g L^{-1}; time: 5 h; T: 22 ± 1 °C; Metal list includes Si metalloid).

playing with the gradient in affinity), and (c) increasing the ionic strength (for displacing the ion-exchange equilibrium). These strategies (and their combination) have been tested for selecting the optimum eluent. Fig. S25 compares the desorption kinetics for both U(VI) and Th(IV) on metal-loaded functionalized silica beads. In the case of Na$_2$CO$_3$ (1 M) eluent, U(VI) desorption is fully achieved within 60 min for TUR/SiO$_2$ and 180 min for UR/SiO$_2$. The ability of uranyl to form strong complexes in the presence of carbonate or bicarbonate may explain the efficiency of this eluent (Kabay et al., 1998; Stopa and Yamaura, 2010). Thorium desorption is less efficient: both the equilibrium time (between 120 and 240 min) and the rate of desorption depend on the sorbent; however, desorption efficiency does not exceed 70%. This is consistent with previous observations on U(VI)/Th(IV) sorption/desorption using graphene oxide/MnO$_2$ composite (Pan et al., 2016), where Pan et al. also observed the differential desorption between U(VI) and Th(IV). Citric acid (1 M) was also tested for the elution of loaded sorbents. The complete desorption is only obtained for U(VI)-loaded UR/SiO$_2$ sorbent (requiring 180–240 min of contact); for the other systems, the equilibrium was reached after 120 min and the desorption efficiency varied between 62% and 78%. Citrate anions are less efficient for complexing U(VI) and Th(IV), making difficult the displacement of metal ions from sorbent surfaces. The release of metal ions is less efficient from thiourea-functionalized silica beads. Similar depreciated desorption for TUR/SiO$_2$ (against UR/SiO$_2$) is also observed for metal desorption using 1 M NaCl/0.1 M H$_2$SO$_4$ eluent: the desorption ranges between 79% and 92% (within 120 min of agitation); while total desorption occurs within 40 min in the case of UR/SiO$_2$ for both U(VI) and Th(IV). However, the best desorption profiles are clearly obtained with more acidic solutions, using 0.5 M HCl solutions: total desorption is achieved within 120 min for Th(IV) elution from TUR/SiO$_2$, while 30 min are sufficient for the other systems (metal ion/sorbent).

Hydrochloric acid was selected for further studies, using a concentration of 0.3 M (for reducing the aggressive strength of the eluent). Fig. S26 compares the kinetics of desorption for the different systems. A remarkable superposition of the profiles is observed. Under selected experimental conditions, 30 min of contact are sufficient for achieving the complete desorption of U(VI) and Th(IV) from UR/SiO$_2$ and TUR/SiO$_2$. The slopes for UR/SiO$_2$ are steeper than those for TUR/SiO$_2$: the thiocarbonyl group contributes to strengthen the interaction with metal ions, making more difficult

the release of bound molecules; this is also consistent with the slower kinetics observed in the sorption step. The desorption kinetics of U(VI) and Th (IV) from sorbents loaded in bi-component solutions is shown in Fig. S27. Full desorption takes place within 60 min of contact. Faster desorption (20–30 min) is observed for U(VI) with UR/SiO$_2$ and Th(IV) with TUR/SiO$_2$; however, these differences are not marked enough for playing on kinetics for improving the separation of U(VI) and Th(IV).

The recycling of the sorbent was tested for five successive sorption/desorption cycles using 0.3 M HCl solutions. Table 1 shows that for both U(VI) and Th(IV) the functionalized silica beads offer remarkable stability in terms of sorption and desorption performances. Desorption efficiency remains systematically higher than 99% along the five runs. A weak and progressive decrease in sorption efficiency is observed. It is noteworthy that the loss in sorption efficiency remains below 4% at the fifth cycle

Table 1

Sorption (SE, %) and desorption (DE, %) efficiencies for five successive recycling steps for UR/SiO$_2$ and TUR/SiO$_2$ for U(VI) and Th(IV) removal.

Sorbent	Run #	U(VI)				Th(IV)			
		SE		DE		SE		DE	
		Aver.	St. dev.	Aver.	St. dev.	Aver.	St. dev.	Aver.	St. dev.
UR/SiO$_2$	1	95.1	1.2	100.4	0.5	63.4	1.1	100.0	0.1
	2	93.7	1.3	99.8	0.1	63.0	1.5	99.8	0.4
	3	93.0	1.1	99.6	0.6	62.2	1.4	100.0	0.2
	4	91.9	1.3	100.0	0.1	61.6	0.9	100.0	0.7
	5	91.2	1.2	99.5	0.3	61.2	1.1	100.0	0.0
Loss (5th/1st)		4.1%				3.5%			
TUR/SiO$_2$	1	75.9	0.6	99.7	0.2	64.5	1.0	100.1	0.2
	2	75.5	0.9	100.0	0.0	63.7	0.9	100.0	0.0
	3	74.8	0.3	99.9	0.3	63.4	1.0	100.0	0.1
	4	74.0	0.5	99.9	0.4	62.7	0.9	100.2	0.5
	5	73.0	0.5	99.7	0.8	62.2	0.8	100.3	0.4
Loss (5th/1st)		3.8%				3.6%			

Metal-loaded samples were collected from uptake kinetics. Demineralized water was used for washing sorbents between each recycling step. Desorption step: SD: 2 g L^{-1}; time: 2 h; T: 22 ± 1 °C; v: 210 rpm.

(compared with initial sorption performance). These levels are consistent with many data reported in the literature (Keshtkar et al., 2013; Liu et al., 2020a; Ma et al., 2020). This performance is much better than for other supports, where the loss in sorption reached up to 20% at the fifth cycle for functionalized porous activated carbon fibres (Mishra et al., 2015), or 15% for functionalized marine fungal biosorbent (Han et al., 2020). This means that the sorption is stable despite the changes observed in FTIR spectra; these chemical modifications (probably associated with protonation of some reactive groups) are not inhibiting the reactivity of functional groups at the surface of silica beads. Since the metals are apparently fully desorbed, the weak decrease in sorption efficiency may be associated with the chemical changes in the polymer coating in both terms of chemistry (functional groups) and physics (possible changes in the porous characteristics, due to pore shrinkage), rather than to the saturation of reactive groups. The FTIR study showed that the spectra were not restored after the fifth desorption step. However, the loss in efficiency remains very limited at the fifth cycle: the sorption performance remains remarkably stable.

3.3. Application to metal recovery from ore leachate

3.3.1. Ore leaching (PLS) and pre-treatment by successive precipitation steps (PPLS)

Table S2 summarizes the characteristics of selected pegmatite ore (major metal oxides and valuable metal traces). The acidic leaching produces pregnant leaching solution (PLS) bearing huge amounts of aluminum ($\sim$13.99 g Al L^{-1}, 0.518 mM), sodium ($\sim$6.28 g Na L^{-1}, 0.273 M), iron ($\sim$3.36 g Fe L^{-1}, 0.06 M), and potassium ($\sim$2.19 g K L^{-1}, 0.056 M). Apart these major elements, which may have competitive effect (especially Al(III) and Fe(III)), the leachates contain important concentrations of calcium ($\sim$0.53 g Ca L^{-1}, 0.013 M), magnesium ($\sim$0.33 g Mg L^{-1}, 0.014 M) and manganese ($\sim$0.13 g Mn L^{-1}, 2.37 mM). The leaching released about 50% of target metals (i.e., U and Th); 69% of Na, 51% of Fe, 30–35% of Al and Mn, about 14% of Mg and K. The limited extraction of U(VI) can be partially explained by the possible presence of uranium under both U(VI) and U(IV) forms.

These high levels of metal ions (potentially competitive) may explain that pre-treatments were processed before testing the sorption properties of functionalized silica beads, in order to decrease their residual concentrations to levels compatible with the sorption process. The first precipitation step was operated at pH 4 to mainly remove Fe(III); the second step at pH 5 drastically reduces the concentration of Al(III). At the end of these successive precipitation steps, their removal yield reached up to 97.5% and 99.2%, respectively: their final concentrations are close to 84 mg Fe L^{-1} (1.50 mmol Fe L^{-1}) and 106 mg Al L^{-1} (3.93 mmol Al L^{-1}). Calcium was also significantly reduced: loss reaches $\sim$40% (residual concentration close to 320 mg Ca L^{-1}, 7.98 mmol Ca L^{-1}). Other elements were reduced by less than 20% with residual concentrations ranging between 111 mg Mn L^{-1} (2.02 mmol Mn L^{-1}) to 277 mg Mg L^{-1} (11.4 mmol Mg L^{-1}). The highest concentrations correspond to K and Na elements (1.79 g K L^{-1} and 6.88 g Na L^{-1}, or 0.046 mmol K L^{-1} and 0.299 mmol Na L^{-1}), which are relatively innocuous for the sorption process. The precipitation steps weakly alter the concentrations of target metals (loss around 20%): 218 mg U L^{-1} (i.e., 0.916 mmol U L^{-1}) and 338 mg Th L^{-1} (1.46 mmol Th L^{-1}). The behavior of other strategic metals, significantly present in the pegmatite, such as REEs, Zr, Hf, and Nb is currently under investigation.

3.3.2. Metal sorption from pre-treated leachates

Section 3.2.4. showed that sorption efficiency and selectivity in multi-component solutions strongly depend on the pH (in the range 1.3–1.5 to 4.8–5.8). Table S17 summarizes the results in the sorption treatment of PPLS using UR/SiO$_2$ and TUR/SiO$_2$ at different pH values (SD: 5 g L^{-1}; time: 5 h). The ranges of sorption efficiencies are reported together with the variation range in sorption capacities. The beneficial effect of pH increase on the recovery of these metals strongly depends on the metal; the most sensitive to pH are Si, Fe and Mg for UR/SiO$_2$ and Si, Fe, U for TUR/SiO$_2$. It is noteworthy that the cumulative sorption capacity reaches 2.08 mmol g^{-1} for UR/SiO$_2$ and 1.73 mmol g^{-1} for TUR/SiO$_2$. The maximum sorption capacities for the recovery of U(VI) and Th(IV) from ore leachate, are very close for the two sorbents: close to 0.177 mmol g^{-1} for U(VI) and 0.275 mmol g^{-1} for Th(IV). These levels are substantially lower than the maximum sorption capacities reported for synthetic single-component solutions: the complexity of the solutions strongly reduces the efficiency of the sorbents for U and Th recovery and the selectivity observed while using synthetic equimolar solutions (Section 3.2.4).

Fig. 8 shows the selectivity coefficients $SC_{U/Metal}$ and $SC_{Th/Metal}$ in function of equilibrium pH for the two sorbents. These profiles are obviously
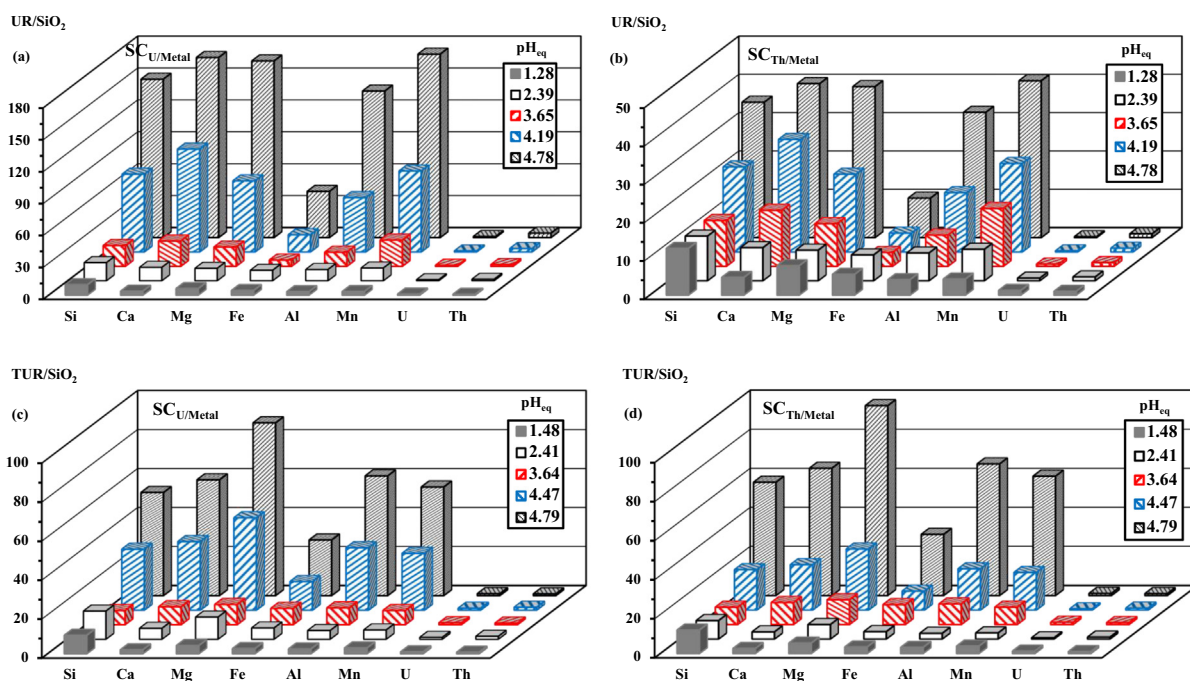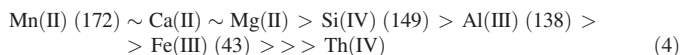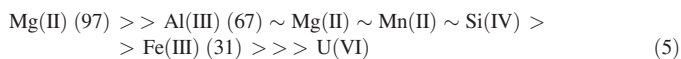

Fig. 8. Recovery of U(VI) and Th(IV) from leachates of Egyptian ore at different pH values for UR/SiO$_2$ – SC coefficients (a: $SC_{U/Metal}$ and b: $SC_{Th/Metal}$) and TUR/SiO$_2$ (c: $SC_{U/Metal}$ and d: $SC_{Th/Metal}$) (SD: 5 g L^{-1}; time: 5 h; T: 22 ± 1 °C; metal list includes Si metalloid).

influenced by the different orders of concentrations of the metals in the PPLS; however, this gives some general trends on the preference of the sorbent for the different metals. This figure confirms the central role of the pH in the selectivity of the sorbent for U and Th. The selectivity of the sorbents increases with pH_{eq}: optimum pH is close to 5. The highest separation of U from other base metals (or metalloid) is obtained at this pH value using UR/SiO_2 according the series:

$$Mn(II)\ (172) \sim Ca(II) \sim Mg(II) > Si(IV)\ (149) > Al(III)\ (138) > \\ > Fe(III)\ (43) > > > Th(IV) \qquad (4)$$

At pH_{eq}: 4.78, $SC_{U/Th}$ reaches 4.2. The sorbent has a marked preference for U(VI) over Th(IV) but not sufficient for achieving the simple and effective separation of the two metals. Much higher levels of selectivity are obtained against base metals; this allows reaching high levels of concentration; the concentration factor (i.e., CF: q_{eq}/C_0, $L\,g^{-1}$) is improved; however, the huge excess of some of these metals makes difficult the selective separation of U(VI) and Th(IV) from base metals.

In the case of thorium separation, the highest selectivity coefficients are found with TUR/SiO_2 at pH_{eq} 5.79, at least against heavy metals (and metalloid); this is probably associated with the occurrence of formation of colloidal species or precipitates. The $SC_{Th/U}$ varies between 0.65 and 1.27; consistently with previous results (Section 3.2.4), TUR/SiO_2 is poorly selective for Th(IV) separation from U(VI). For heavy metals (or metalloid), the $SC_{Th/Metal}$ values can be ranked according:

$$Mg(II)\ (97) > > Al(III)\ (67) \sim Mg(II) \sim Mn(II) \sim Si(IV) > \\ > Fe(III)\ (31) > > > U(VI) \qquad (5)$$

The plots of $\log_{10} D$ vs. pH_{eq} (Fig. S28) follow similar trends as those reported in the study of U(VI) and Th(IV) sorption from multi-component equimolar solutions (Fig. S16). The linear plots for U(VI) and Th(IV) are shifted toward higher distribution ratio compared with those of other metals: the sorbents show significant preference for U(VI) and Th(IV) against base metals. UR/SiO_2 remains more efficient for U(VI) binding (preference against Th(IV)); on the opposite hand, in the case of TUR/SiO_2, the distribution ratios are almost overlapped for the two actinides.

Fig. S29 shows the semi-quantitative EDX analysis of the sorbents after the treatment of PPLS at pH 5. The data show that the sorbent have roughly the same metal contents. The presence of S element at remarkable level also for UR/SiO_2 (free of S-groups) means that the sorbent also binds S and P elements (probably as free species or as metal-complexed forms).

3.3.3. Metal desorption from sorbents and treatment of eluates

The elution of the metals from sorbents loaded from PPLS at pH_0: 5 was performed using 0.5 M HCl solution. Table S18 demonstrates the highly effective desorption of the metals; the data report the average values (and relevant standard deviations) for the results collected at different pH values for leachates treatment (pH_0: 1–5). In most cases, the desorption yield exceeds 96%, the weaker elution levels are reported for Fe(III) and Al(III) (desorption yields between 92% and 95%). As expected, since the metal sorption increased with the pH, the levels of metals in the eluates vary according pH. Table S18 shows the concentrations obtained specifically with the sorbents loaded at pH_0 5. The concentrations of U(VI) and Th (IV) reach comparable values: 605–585 mg U L^{-1} (2.54–2.46 mmol U L^{-1}) and 895–911 mg Th L^{-1} (3.86–3.93 mmol Th L^{-1}) in the eluates produced from both UR/SiO_2 and TUR/SiO_2. These levels are significantly higher than those obtained with the other metals. This is consistent with the preference of the sorbents for U and Th and with the concentration factors reported above.

The separation of thorium may be processed using oxalate precipitation method. Indeed, in acidic solutions, the weak solubility of thorium in the presence of oxalate (Kobayashi et al., 2009) makes possible the selective precipitation of Th(IV) from U(VI) and base metals (Abd El Fatah, 2020). Tables S19 and S20 report the precipitation efficiency of the different metals in the presence of oxalic acid (15%, w/w) at pH ~1.1. All the metals

are precipitated with yields ranging between 14% and 21% for UR/SiO_2 and 14–29% for TUR/SiO_2, except thorium that was almost completely recovered by oxalate precipitation (~96%). The semi-quantitative EDX analysis shows the thorium oxalate cake contains traces of chlorine, iron and uranium (total: ~4.3%, weight percentage; 2.1–3.3, atomic percentage). The process allows recovering relatively pure thorium salt that could be calcined to produce thorium oxide.

After the precipitation of thorium, a new precipitation step (at pH ~9) allows recovering uranyl hydroxide (recovery efficiency: ~97.7%). Other metal ions are also precipitated with yields around 21–28% (up to 34–25%, for thorium). However, the relatively low concentrations of the metals in the residue of oxalate precipitation step may explain that the semi-quantitative analysis (Fig. S30) shows that the U cake contains about 8–10% of impurities (as Cl, Na, Fe, Ca, Al, Mg, and Th, 8–9%, in atomic percentage).
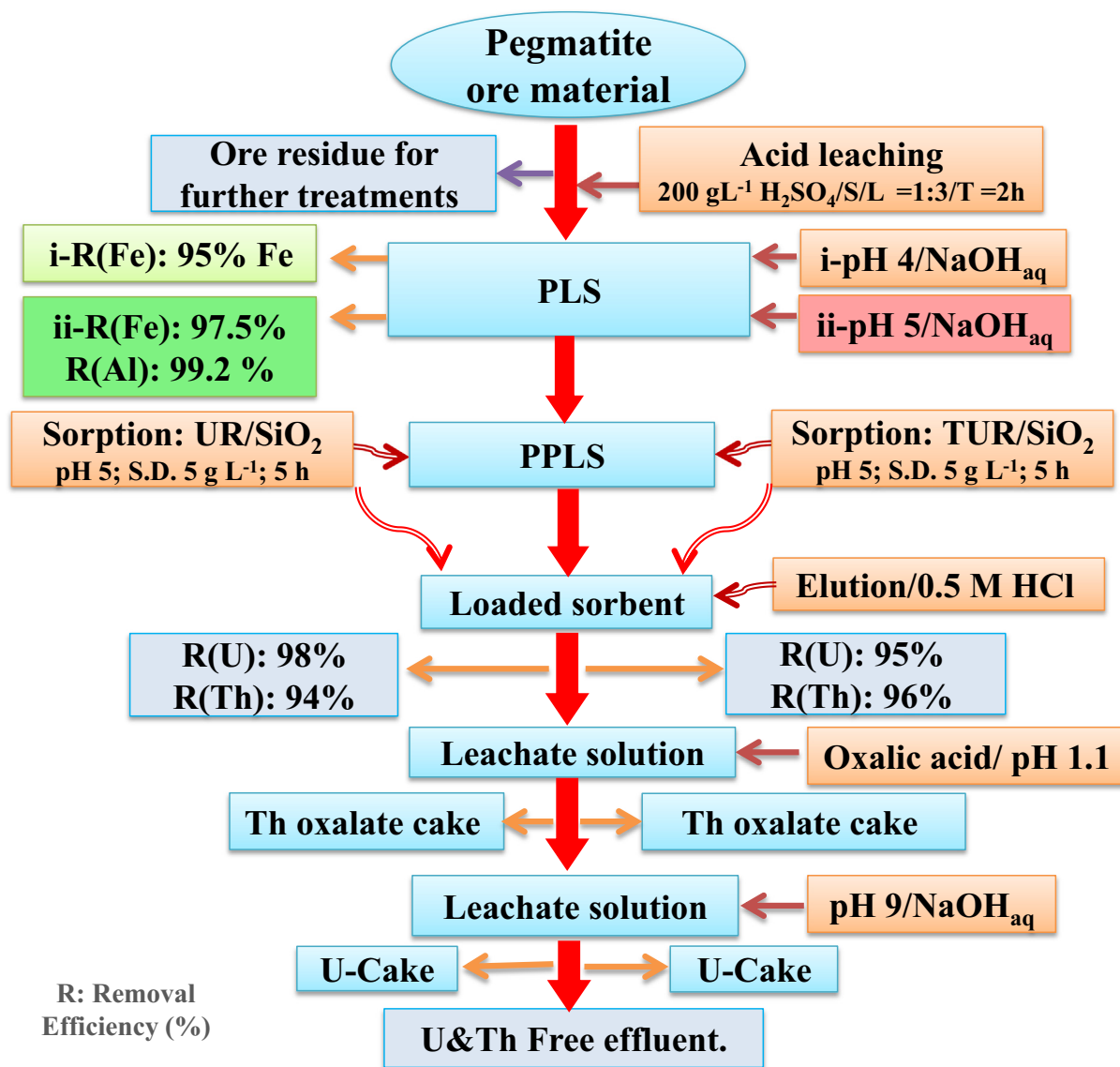
A series of washing steps (using deionized water) was performed to remove most of the soluble ions such as Cl^-, Na^+, and Mg^{2+}; the concentration of the other co-ions was significantly reduced consequently to the dilution effect.

3.3.4. Proposed flowsheet

Scheme 3 shows suggested flow sheet for the treatment of pegmatite ore. Fig. 9 reports the distribution of selected metals for the two types of sorbents within the different compartments: ore residue (after leaching), different precipitates for the pre-treatment of PLS, residual solution after sorption step, residue on the sorbent after elution step, thorium-cake (after oxalate precipitation), uranium-cake (after alkaline precipitation) and residual final solution. The two profiles of distribution are very similar showing the global reproducibility (consistent with the relatively close sorption behavior of UR/SiO_2 and TUR/SiO_2). First, Si(IV) is not represented, the leaching process was ineffective for solubilizing this metalloid. The leaching step is poorly efficient for Ca(II) and Mg(II): 85–95% of these alkali-earth elements remains in the ore; this is favorable for decreasing the competitive effect for the sorption of target elements. For base metals (including Fe(III), Al(III) and Mn(II)), the extraction ranges between 30% and 50%. Most of leached iron is precipitated at pH 4 (more than 97% is assigned to the residual ore and the pH 4 precipitate); a residual amount (corresponding to ~1.4%) is collected in the pH 5 precipitate. In the case of Al, about 99.8% is localized in the residual ore (~68.5%), the pH 5 precipitate (~24.1%), and the pH 4 precipitate (~7.2%). For Mn, the treated ore still contains 65.6% of total element, while very low amounts are successively precipitated (about 4.7%). A substantial fraction (~21.5%) is passing through the sorption step (collected in the residue); while most of the remaining fraction (~5.1%) is collected in the final residue (after U-cake formation; 3.1% of total Mn is distributed in the other compartments as traces). The leaching process has a global efficiency relatively low (about 50%) for target metals (i.e., U and Th); however, the combination of leaching and pre-treatment of leachates allows the efficient separation of competitor metal ions for improving the efficiency of the sorption process of valuable metals. Indeed, for uranium, the leaching process released about 55% of the metal, while the precipitation steps lose about 11.4% of U(VI). About 5.8% of U(VI) is co-precipitated in the Th-cake; however, most of uranium is recovered in the U-cake (34.5–35.8%) (traces, less than 3%, can be found in the other compartments). The leaching of thorium is less efficient (representing only 45.6%); however, a lower fraction of the metal is lost in the successive precipitation pre-treatments (less than 9%). The separation of the metal in the Th-cake is highly effective: ~32.9–33.3% of total Th; while residual Th(IV) can be collected in the residue of sorption operation (1.56–2.22%) and in the final aqueous solution (i.e., ~1%). It is noteworthy that the U-cake contains negligible fraction of Th (around 0.4% of total Th).

4. Conclusion

The functionalization of silica beads with the surface deposition of formaldehyde-crosslinked urea (or thiourea) allows preparing efficient

Scheme 3 Flowsheet

```
                    ┌─────────────────────┐
                    │   Pegmatite         │
                    │   ore material      │
                    └─────────────────────┘
                              │
┌──────────────────────┐     │     ┌─────────────────────────────────────┐
│ Ore residue for      │◄────┼─────│ Acid leaching                       │
│ further treatments   │     │     │ 200 gL⁻¹ H₂SO₄/S/L =1:3/T =2h       │
└──────────────────────┘     ▼     └─────────────────────────────────────┘
┌──────────────────────┐                              ┌─────────────────────────┐
│ i-R(Fe): 95% Fe      │◄──┐  ┌─────────┐  ┌──────────│ i-pH 4/NaOH_aq          │
└──────────────────────┘   └──│  PLS    │──┘           └─────────────────────────┘
┌──────────────────────┐      │         │              ┌─────────────────────────┐
│ ii-R(Fe): 97.5%      │◄─────│         │◄─────────────│ ii-pH 5/NaOH_aq         │
│ R(Al): 99.2 %        │      └─────────┘              └─────────────────────────┘
└──────────────────────┘           │
┌──────────────────────┐           ▼
│ Sorption: UR/SiO₂    │      ┌─────────┐      ┌──────────────────────────┐
│ pH 5; S.D. 5 g L⁻¹; 5 h│──►│  PPLS   │◄─────│ Sorption: TUR/SiO₂       │
└──────────────────────┘      └─────────┘      │ pH 5; S.D. 5 g L⁻¹; 5 h  │
                                   │           └──────────────────────────┘
                                   ▼
                         ┌───────────────────┐      ┌─────────────────────┐
                         │ Loaded sorbent    │◄─────│ Elution/0.5 M HCl   │
                         └───────────────────┘      └─────────────────────┘
┌──────────────┐                 │                  ┌──────────────┐
│ R(U): 98%    │◄────────────────┼─────────────────►│ R(U): 95%    │
│ R(Th): 94%   │                 ▼                  │ R(Th): 96%   │
└──────────────┘       ┌───────────────────┐        └──────────────┘
                       │ Leachate solution │◄──┐ ┌─────────────────────┐
                       └───────────────────┘   └─│ Oxalic acid/ pH 1.1 │
┌──────────────────┐         │                   └─────────────────────┘
│ Th oxalate cake  │◄────────┼────────►┌──────────────────┐
└──────────────────┘         ▼         │ Th oxalate cake  │
                   ┌───────────────────┘└──────────────────┘
                   │ Leachate solution │◄──┐ ┌──────────────────┐
                   └───────────────────┘   └─│ pH 9/NaOH_aq     │
┌──────────┐             │                   └──────────────────┘
│ U-Cake   │◄────────────┼────────►┌──────────┐
└──────────┘             ▼         │ U-Cake   │
                 ┌───────────────────┘└──────────┘
                 │ U&Th Free effluent. │
                 └─────────────────────┘
```

R: Removal Efficiency (%)

Scheme 3. Flowsheet for the recovery and separation of U(VI) and Th(IV) (yields are referred to metal contents in the PLS and/or PPLS compartments).

sorbents containing up to 7.8 mmol N g^{-1} (and for thiourea, up to 1.5 mmol S g^{-1}). These amine groups, combined with carbonyl (or thiocarbonyl) groups may explain the good sorption properties for U(VI) and Th(IV). These sorption properties are significantly higher than those obtained for pristine silica beads. At optimized pH (i.e., ~4–5), the deprotonation of reactive groups and the speciation of metal ions improve the sorption capacities that can reach sorption capacities as high as 1–1.2 mmol g^{-1} (remarkable values taking into account the relative weight fraction of silica support; i.e., 55–60%). Sorption isotherms (performed at pH_0 4, to prevent any risk of metal precipitation at high concentration) are described by the Langmuir equation. The study of the effect of temperature on the sorption of metal ions shows that sorption is endothermic for UR/SiO₂ and exothermic for TUR/SiO₂, as a complementary proof of the difference in sorption mechanisms. The small size of functionalized beads (110–130 μm in diameter) minimizes the resistance to intraparticle diffusion (which cannot be neglected); the kinetic profiles are fitted by the pseudo-first order rate equation and the equilibrium time in close to 60–90 min.

The sorption of U(VI) and Th(IV) in multi-component solutions shows a remarkable preference for U(VI) > Th(IV) against base metals, alkali-earth metals and Si metalloid at pH_{eq} close to 5, especially for UR/SiO₂. For TUR/SiO₂, the thiocarbonyl group brings new reactive groups with broader

reactivity, and consequently lower selectivity. The separation of U(VI) from Th(IV) reveals difficult: the selectivity coefficients are relatively close and UR/SiO₂ has a little preference for U(VI) against Th(IV), while the trend is reversed for TUR/SiO₂. Acidic solutions (0.3–0.5 M HCl) are highly efficient for the elution of sorbed metal ions; the total desorption is achieved within 30–60 min and the sorbent can be recycled for at least five times with complete desorption and relatively stable sorption efficiency (the loss in efficiency being less than 4% at the fifth cycle).

The acidic leaching of pegmatite ore produces a very complex effluent containing huge amounts of competitor metals. However, the combination of leaching with pre-treatment steps allows producing a leachate with more appropriate concentrations; this makes possible the efficient sorption of target metals. Combined with elution and a series of selective precipitation steps (successively: oxalate and alkaline), thorium- and uranium-cakes can be obtained with relatively high purity.

The easy synthesis of urea-functionalized silica beads shows promising performances for the recovery of uranium and thorium, even when applied to complex solutions. The coating of silica beads strongly increases sorption properties; the support mainly contributes to improving the mechanical stability of the material, enhances the specific surface area (compared with bulk polymer) and would facilitate the application of the sorbents in fixed-bed columns.
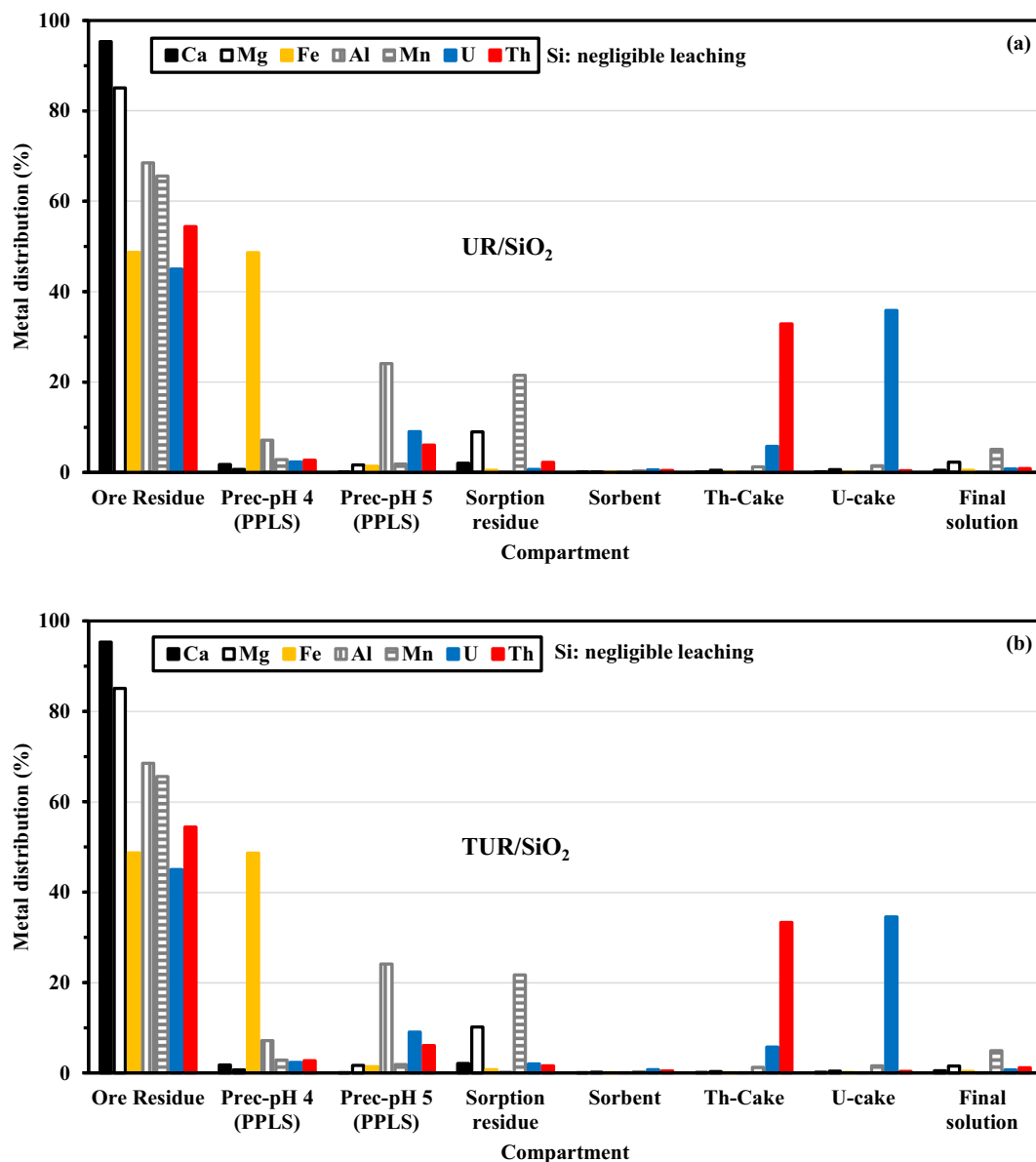
Fig. 9. Distribution of selected metals (or metalloid) along the extraction process summarized in Scheme 2 for UR/SiO$_2$ (a) and TUR/SiO$_2$ (b) sorbents (Si element being negligibly leached is not represented in the figure; the values of metal distribution are referred to total contents in the ore; reported data concern the experiments performed with the sorption step at pH$_0$: 5).

Appendix A. Supplementary data

Supplementary data to this article can be found online at https://doi.org/10.1016/j.scitotenv.2022.153184.

References

Abd El Fatah, A.I.L., 2020. Commercial approach for highly pure thorium from Egyptian monazite mineral acid process. 10th International Conference on Chemical and Environmental Engineering (ICEE-10). 975. IOPScience, Military Technical College, Kobry El-Kobbah, Cairo, Egypt Art. N° 012022.

Abdel Raouf, M.W., El-Kamash, A.M., 2006. Kinetics and thermodynamics of the sorption of uranium and thorium ions from nitric acid solutions onto a TBP-impregnated sorbent. J. Radioanal. Nucl. Chem. 267, 389–395.

Abhilash, Pandey, B.D., 2013. Microbially assisted leaching of uranium: a review. Miner. Process. Extr. Metall. Rev. 34, 81–113.

Ahmed, W., Mehmood, S., Núñez-Delgado, A., Qaswar, M., Ali, S., Ying, H., et al., 2021. Fabrication, characterization and U(VI) sorption properties of a novel biochar derived from Tribulus terrestris via two different approaches. Sci. Total Environ. 780, 146617.

Alothman, Z.A., 2012. A review: fundamental aspects of silicate mesoporous materials. Materials 5, 2874–2902.

Amesh, P., Suneesh, A.S., Venkatesan, K.A., Chandra, M., Ravindranath, N.A., 2020. High capacity amidic succinic acid functionalized mesoporous silica for the adsorption of uranium. 602, 125053.

Amesh, P., Venkatesan, K.A., Suneesh, A.S., Samanta, N., 2020b. Diethylenetriamine tethered mesoporous silica for the sequestration of uranium from aqueous solution and seawater. J. Environ. Chem. Eng. 8, 103995.

Ang, K.L., Li, D., Nikoloski, A.N., 2017. The effectiveness of ion exchange resins in separating uranium and thorium from rare earth elements in acidic aqueous sulfate media. Part 1. Anionic and cationic resins. Hydrometallurgy 174, 147–155.

Ang, K.L., Li, D., Nikoloski, A.N., 2018. The effectiveness of ion exchange resins in separating uranium and thorium from rare earth elements in acidic aqueous sulfate media. Part 2. Chelating resins. Miner. Eng. 123, 8–15.

Atta, A.M., Akl, Z.F., 2015. Removal of thorium from water using modified magnetite nanoparticles capped with rosin amidoxime. Mater. Chem. Phys. 163, 253–261.

Atta, A.M., Al-Lohedan, H.A., Tawfik, A.M., Ezzat, A.O., 2016. Application of superamphiphilic silica-nanogel composites for fast removal of water pollutants. Molecules 21, 1392.

Barbette, F., Rascalou, F., Chollet, H., Babouhot, J.L., Denat, F., Guilard, R., 2004. Extraction of uranyl ions from aqueous solutions using silica-gel-bound macrocycles for alpha contaminated waste water treatment. Anal. Chim. Acta 502, 179–187.

Bayramoglu, G., Arica, M.Y., 2016. MCM-41 silica particles grafted with polyacrylonitrile: modification in to amidoxime and carboxyl groups for enhanced uranium removal from aqueous medium. Microporous Mesoporous Mater. 226, 117–124.

Bleise, A., Danesi, P.R., Burkart, W., 2003. Properties, use and health effects of depleted uranium (DU): a general overview. J. Environ. Radioact. 64, 93–112.

Borai, E.H., Abd El-Ghany, M.S., Ahmed, I.M., Hamed, M.M., El-Din, A.M.S., Aly, H.F., 2016. Modified acidic leaching for selective separation of thorium, phosphate and rare earth concentrates from Egyptian crude monazite. Int. J. Miner. Process. 149, 34–41.

Cheira, M.F., 2020. Synthesis of aminophosphonate-functionalised ZnO/polystyrene-butadiene nanocomposite and its characteristics for uranium adsorption from phosphoric acid. Int. J. Environ. Anal. Chem. 101, 1710–1734.

Chen, C., Wang, X., 2007. Sorption of Th (IV) to silica as a function of pH, humic/fulvic acid, ionic strength, electrolyte type. Appl. Radiat. Isot. 65, 155–163.

Chen, C.L., Li, X.L., Wang, X.K., 2007. Application of oxidized multi-wall carbon nanotubes for Th(IV) adsorption. Radiochim. Acta 95, 261–266.

Chen, A., Shang, C., Shao, J., Zhang, J., Huang, H., 2017. The application of iron-based technologies in uranium remediation: a review. Sci. Total Environ. 575, 1291–1306.

Dabbagh, R., Rojaee, A., Heshmatipour, Z., 2018. Thermodynamics, kinetics, and equilibrium studies of uranium sorption by Gracilaria corticata red alga. Environ. Eng. Manag. J. 17, 1199–1208.

Davies, W., Gray, W., 1964. A rapid and specific titrimetric method for the precise determination of uranium using iron(II) sulphate as reductant. Talanta 11, 1203–1211.

El-Magied, M.O.A., Dhmees, A.S., Abd El-Hamid, A.A.M., Eldesouky, E.M., 2018. Uranium extraction by sulfonated mesoporous silica derived from blast furnace slag. J. Nucl. Mater. 509, 295–304.

Elwakeel, K.Z., Shahat, A., Al-Bogami, A.S., Wijesiri, B., Goonetilleke, A., 2020. The synergistic effect of ultrasound power and magnetite incorporation on the sorption/desorption behavior of Cr(VI) and As(V) oxoanions in an aqueous system. J. Colloid Interface Sci. 569, 76–88.

Ertan, E., Guelfen, M., 2009. Separation of gold(III) ions from copper(II) and zinc(II) ions using thiourea-formaldehyde or urea-formaldehyde chelating resins. J. Appl. Polym. Sci. 111, 2798–2805.

Esen Erden, K., Donat, R., 2017. Removal of thorium(IV) from aqueous solutions by natural sepiolite. Radiochim. Acta 105, 187–196.

Gabriel, S., Baschwitz, A., Mathonniere, G., Eleouet, T., Fizaine, F., 2013. A critical assessment of global uranium resources, including uranium in phosphate rocks, and the possible impact of uranium shortages on nuclear power fleets. Ann. Nucl. Energy 58, 213–220.

Gezer, N., Gulfen, M., Aydin, A.O., 2011. Adsorption of selenite and selenate ions onto thiourea-formaldehyde resin. J. Appl. Polym. Sci. 122, 1134–1141.

Giannakoudakis, D.A., Anastopoulos, I., Barczak, M., Alphantoniou, E., Terpilowski, K., Mohammadi, E., et al., 2021. Enhanced uranium removal from acidic wastewater by phosphonate-functionalized ordered mesoporous silica: surface chemistry matters the most. J. Hazard. Mater. 413, 125279.

Gladysz-Plaska, A., Grabias, E., Majdan, M., 2018. Simultaneous adsorption of uranium(VI) and phosphate on red clay. Prog. Nucl. Energy 104, 150–159.

Gómez, D.E., Fabbrizzi, L., Licchelli, M., Monzani, E., 2005. Urea vs. thiourea in anion recognition. Org. Biomol. Chem. 3, 1495–1500.

Guo, X., Feng, Y., Ma, L., Gao, D., Jing, J., Yu, J., et al., 2017. Phosphoryl functionalized mesoporous silica for uranium adsorption. Appl. Surf. Sci. 402, 53–60.

Hadjittofi, L., Pashalidis, I., 2014. Uranium sorption from aqueous solutions by activated biochar fibres investigated by FTIR spectroscopy and batch experiments. J. Radioanal. Nucl. Chem. 304, 897–904.

Hamza, M.F., 2019. Grafting of quaternary ammonium groups for uranium(VI) recovery: application on natural acidic leaching liquor. J. Radioanal. Nucl. Chem. 322, 519–532.

Hamza, M.F., El-Aassy, I.E., Guibal, E., 2019. Integrated treatment of tailing material for the selective recovery of uranium, rare earth elements and heavy metals. Miner. Eng. 133, 138–148.

Hamza, M.F., Fouda, A., Elwakeel, K.Z., Wei, Y., Guibal, E., Hamad, N.A., 2021. Phosphorylation of guar gum/magnetite/chitosan nanocomposites for uranium (VI) sorption and antibacterial applications. Molecules 26, 1920.

Han, J., Hu, L., He, L., Ji, K., Liu, Y., Chen, C., et al., 2020. Preparation and uranium (VI) biosorption for tri-amidoxime modified marine fungus material. Environ. Sci. Pollut. Res. 27, 37313–37323.

Hao, Z., Guo, Y., Wu, P., Mansuer, M., Zhu, J., 2014. Adsorption properties of silver ions on thiourea-formaldehyde resin. In: Pan, W., Xu, Q.J., Li, H. (Eds.), Exploration and Processing of Mineral Resources. 868, pp. 459–462.

Hu, B., Hu, Q., Chen, C., Sun, Y., Xu, D., Sheng, G., 2017. New insights into Th(IV) speciation on sepiolite: evidence for EXAFS and modeling investigation. Chem. Eng. J. 322, 66–72.

Hubbe, M.A., Azizian, S., Douven, S., 2019. Implications of apparent pseudo-second-order adsorption kinetics onto cellulosic materials: a review. Bioresources 14, 7582–7626.

Ismail, L.S., Khalili, F.I., Abu Orabi, F.M., 2020. Thorium(IV) removal and recovery from aqueous solutions using modified silica nanoparticles with cysteine or methionine amino acids. Desalin. Water Treat. 196, 161–176.

Kabay, N., Demircioglu, M., Yayli, S., Gunay, E., Yuksel, M., Saglam, M., et al., 1998. Recovery of uranium from phosphoric acid solutions using chelating ion-exchange resins. Ind. Eng. Chem. Res. 37, 1983–1990.

Kamal, E., Hamdy, G., El-Sabbagh, I.A., 2021. Highly efficient capture of Th(IV) from aqueous solutions using GO/TiO2 nanocomposite. Egypt. J. Chem. 64, 1353–1362.

Keshtkar, A.R., Irani, M., Moosavian, M.A., 2013. Removal of uranium (VI) from aqueous solutions by adsorption using a novel electrospun PVA/TEOS/APTES hybrid nanofiber membrane: comparison with casting PVA/TEOS/APTES hybrid membrane. J. Radioanal. Nucl. Chem. 295, 563–571.

Kirci, S., Guelfen, M., Aydin, A.O., 2009. Separation and recovery of silver(I) ions from base metal ions by thiourea- or urea-formaldehyde chelating resin. Sep. Sci. Technol. 44, 1869–1883.

Kobayashi, T., Sasaki, T., Takagi, I., Moriyama, H., 2009. Solubility of thorium(IV) in the presence of oxalic and malonic acids. J. Nucl. Sci. Technol. 46, 1085–1090.

Kouraim, M.N., Hagag, M.S., Ali, A.H., 2019. Sorption of uranium from radioactive wastes by silicate-neutralised polyacrylic. Int. J. Environ. Anal. Chem. 100, 825–840.

Kursunoglu, S., Hussaini, S., Top, S., Ichlas, Z.T., Gokcen, H.S., Ozsarac, S., et al., 2021. Production of mixed rare earth oxide powder from a thorium containing complex bastnasite ore. Powder Technol. 379, 641–654.

Li, J., Zhang, Y., Zhou, Y., Fang, F., Li, X., 2021. Tailored metal-organic frameworks facilitate the simultaneously high-efficient sorption of $UO2_2+$ and $ReO4−$ in water. Sci. Total Environ. 799: Art. No 149468.

Liao, R., Shi, Z., Hou, Y., Zhang, K., Zhang, J., Wang, X., et al., 2019. Uranium sorption onto mullite: characteristics of isotherms, kinetics and thermodynamics. J. Earth System Science 128, 176.

Liu, H.-J., Jing, P.-F., Liu, X.-Y., Du, K.-J., Sun, Y.-K., 2016. Synthesis of beta-cyclodextrin functionalized silica gel and its application for adsorption of uranium(VI). J. Radioanal. Nucl. Chem. 310, 263–270.

Liu, S., Yang, Y., Liu, T., Wu, W., 2017. Recovery of uranium(VI) from aqueous solution by 2-picolylamine functionalized polystyrene-co-maleic anhydride) resin. J. Colloid Interface Sci. 497, 385–392.

Liu, S., Luo, J., Ma, J., Li, J., Li, S., Meng, L., et al., 2020. Removal of uranium from aqueous solutions using amine-functionalized magnetic platelet large-pore SBA-15.

Liu, X., Hu, S., Xu, D., Shao, D., 2020b. Removal of U(VI) from aqueous solution using carboxymethyl cellulose-modified ca-rectorite hybrid composites. Korean J. Chem. Eng. 37, 776–783.

Liu, Y., Huo, Y., Wang, X., Yu, S., Ai, Y., Chen, Z., et al., 2021a. Impact of metal ions and organic ligands on uranium removal properties by zeolitic imidazolate framework materials. J. Clean. Prod. 278, 123216.

Liu, Y., Pang, H., Wang, X., Yu, S., Chen, Z., Zhang, P., et al., 2021b. Zeolitic imidazolate framework-based nanomaterials for the capture of heavy metal ions and radionuclides: a review. Chem. Eng. J. 406, 127139.

Lopez-Ramon, M.V., Stoeckli, F., Moreno-Castilla, C., Carrasco-Marin, F., 1999. On the characterization of acidic and basic surface sites on carbons by various techniques. Carbon 37, 1215–1221.

Ma, D., Wei, J., Zhao, Y., Chen, Y., Tang, S., 2020. The removal of uranium using novel temperature sensitive urea-formaldehyde resin: adsorption and fast regeneration. Sci. Total Environ. 735, 139399.

Marcus, Y., 1997. Ion properties. Marcel Dekker Inc, New York, NY.

Marczenko, Z., Balcerzak, M., 2000. Chapter 39 - rare-earth elements. In: Marczenko, Z., Balcerzak, M. (Eds.), Analytical Spectroscopy Library. 10. Elsevier, pp. 341–349.

Mathew, K.J., Buerger, S., Vogt, S., Mason, P., Morales-Arteaga, M.E., Narayanan, U.I., 2009. Uranium assay determination using davies and gray titration: an overview and implementation of GUM for uncertainty evaluation. J. Radioanal. Nucl. Chem. 282, 939–944.

Merdivan, M., Duz, M.Z., Hamamci, C., 2001. Sorption behaviour of uranium(VI) with N, N-dibutyl-N '-benzoylthiourea impregnated in amberlite XAD-16. Talanta 55, 639–645.

Mishra, S., Dwivedi, J., Kumar, A., Sankararamakrishnana, N., 2015. Studies on salophen anchored micro/meso porous activated carbon fibres for the removal and recovery of uranium. RSC Adv. 5, 33023–33036.

Mosleh, M.A., El-Hakim, E.H., Ahmed, A.Z., Abd El-Ghany, M.S., El-Didamony, A.M., 2020. Equilibrium and kinetic studies on uranium sorption from aqueous sulphate medium using tri-n-octylamine impregnated resin.

Moulin, C., Amekraz, B., Hubert, S., Moulin, V., 2001. Study of thorium hydrolysis species by electrospray-ionization mass spectrometry. Anal. Chim. Acta 441, 269–279.

Muslu, N., Gulfen, M., 2011. Selective separation and concentration of Pd(II) from Fe(III), Co (II), Ni(II), and Cu(II) ions using thiourea-formaldehyde resin. J. Appl. Polym. Sci. 120, 3316–3324.

Nuhanovic, M., Grebo, M., Draganovic, S., Memic, M., Smjecanin, N., 2019. Uranium(VI) biosorption by sugar beet pulp: equilibrium, kinetic and thermodynamic studies. J. Radioanal. Nucl. Chem. 322, 2065–2078.

Orabi, A.H., 2019. Synthesis of a cellulose derivative for enhanced sorption and selectivity of uranium from phosphate rocks prior to its fluorometric determination. Int. J. Environ. Anal. Chem. 99, 741–766.

Orabi, A., Atrees, M., Salem, H., 2018. Selective preconcentration of uranium on chitosan stearoyl thiourea prior to its spectrophotometric determination. Sep. Sci. Technol. 53, 2267–2283.

Ozudogru, Y., Merdivan, M., 2020. Adsorption of U(VI) and Th(IV) ions removal from aqueous solutions by pretreatment with Cystoseira barbata. J. Radioanal. Nucl. Chem. 323, 595–603.

Pan, N., Li, L., Ding, J., Li, S.K., Wang, R.B., Jin, Y.D., et al., 2016. Preparation of graphene oxide-manganese dioxide for highly efficient adsorption and separation of Th(IV)/U (VI). J. Hazard. Mater. 309, 107–115.

Pearson, R.G., 1966. Acids and bases. Science (New York, N.Y.) 151, 172–177.

Persson, I., 2010. Hydrated metal ions in aqueous solution: how regular are their structures? Pure Appl. Chem. 82, 1901–1917.

Rosenberg, E., Pinson, G., Tsosie, R., Tutu, H., Cukrowska, E., 2016. Uranium remediation by ion exchange and sorption methods: a critical review. Johnson Matthey Technology Review. 60, pp. 59–77.

RSC, 2020. In: RSC (Ed.), Periodic Table. RSC, London (UK) . https://www.rsc.org/periodic-table/.

Sarafraz, H., Minuchehr, A., Alahyarizadeh, G., Rahimi, Z., 2017. Synthesis of enhanced phosphonic functional groups mesoporous silica for uranium selective adsorption from aqueous solutions. Sci. Rep. 7, 11675.

Sheng, G., Hu, J., Wang, X., 2008. Sorption properties of Th(IV) on the raw diatomite—effects of contact time, pH, ionic strength and temperature. Appl. Radiat. Isot. 66, 1313–1320.

Smirnov, A.L., Titova, S.M., Rychkov, V.N., Bunkov, G.M., Semenishchev, V.S., Kirillov, E.V., et al., 2017. Study of scandium and thorium sorption from uranium leach liquors. J. Radioanal. Nucl. Chem. 312, 277–283.

Stopa, L.C.B., Yamaura, M., 2010. Uranium removal by chitosan impregnated with magnetite nanoparticles: adsorption and desorption. Int. J. Nucl. Energy Sci. Technol. 5, 283–289.

Sun, Z., Xiao, Y., Agterhuis, H., Sietsma, J., Yang, Y., 2016. Recycling of metals from urban mines - a strategic evaluation. J. Clean. Prod. 112, 2977–2987.

Swain, N., Mishra, S., 2019. A review on the recovery and separation of rare earths and transition metals from secondary resources. J. Clean. Prod. 220, 884–898.

Tran, H.N., Lima, E.C., Juang, R.-S., Bollinger, J.-C., Chao, H.-P., 2021. Thermodynamic parameters of liquid–phase adsorption process calculated from different equilibrium constants related to adsorption isotherms: a comparison study. J. Environ.Chem. Eng. 9 (6), 106674.

Tuzen, M., Sari, A., Saleh, T.A., 2020. Synthesis, characterization and evaluation of carbon nanofiber modified-polymer for ultra-removal of thorium ions from aquatic media. Chem. Eng. Res. Des. 163, 76–84.

Wamba, A.G.N., Kofa, G.P., Koungou, S.N., Thue, P.S., Lima, E.C., dos Reis, G.S., et al., 2018. Grafting of amine functional group on silicate based material as adsorbent for water purification: a short review. J. Environ. Chem.Eng. 6, 3192–3203.

Wang, Y., Li, Y., Li, L., Kong, F., Lin, S., Wang, Z., et al., 2020. Preparation of three-dimensional fiber-network chitosan films for the efficient treatment of uranium-contaminated effluents. Water Sci. Technol. 81, 52–61.

Wang, Y., Hu, X., Liu, Y., Li, Y., Lan, T., Wang, C., et al., 2021. Assembly of three-dimensional ultralight poly(amidoxime)/graphene oxide nanoribbons aerogel for efficient removal of uranium(VI) from water samples. Sci. Total Environ. 765, 142686.

Wiberg, K.B., Wang, Y.G., 2011. A comparison of some properties of C=O and C=S bonds. ARKIVOC 45–56.

Wu, Z., Yuan, W., Li, J., Wang, X., Liu, L., Wang, J., 2017. A critical review on the recycling of copper and precious metals from waste printed circuit boards using hydrometallurgy. Front. Environ. Sci. Eng. 11, 1–14.

Wu, S., Wang, L., Zhang, P., El-Shall, H., Moudgil, B., Huang, X., et al., 2018. Simultaneous recovery of rare earths and uranium from wet process phosphoric acid using solvent extraction with D2EHPA. Hydrometallurgy 175, 109–116.

Xiao, J., Jing, Y., Wang, X.Q., Yao, Y., Jia, Y.Z., 2018. Preconcentration of uranium(VI) from aqueous solution by amidoxime-functionalized microspheres silica material: kinetics, isotherm and mechanism study. Chemistryselect 3, 12346–12356.

Xie, Y., Chen, C.L., Ren, X.M., Wang, X.X., Wang, H.Y., Wang, X.K., 2019. Emerging natural and tailored materials for uranium-contaminated water treatment and environmental remediation. Prog. Mater. Sci. 103, 180–234.

Yang, Z., Chen, G., Weng, H., Shen, W., Huang, Z., Lin, M., 2018. Efficient and selective separation of U(VI) and Th(IV) from rare earths using functionalized hierarchically mesoporous silica. J. Mater. Sci. 53, 3398–3416.

Yang, P.P., Liu, Q., Liu, J.Y., Chen, R.R., Li, R.M., Bai, X.F., et al., 2019. Highly efficient immobilization of uranium(VI) from aqueous solution by phosphonate-functionalized dendritic fibrous nanosilica (DFNS). J. Hazard. Mater. 363, 248–257.

Yilmaz, C.E., Aslani, M.A.A., Aslani, C.K., 2020. Removal of thorium by modified multi-walled carbon nanotubes: optimization, thermodynamic, kinetic, and molecular dynamic viewpoint. Prog. Nucl. Energy 127, 103445.

Yin, X.J., Bai, J., Fan, F.L., Cheng, W.W., Tian, W., Wang, Y., et al., 2015. Amidoximed silica for uranium(VI) sorption from aqueous solution. J. Radioanal. Nucl. Chem. 303, 2135–2142.

Yin, X., Bai, J., Tian, W., Li, S., Wang, J., Wu, X., et al., 2017. Uranium sorption from saline lake brine by amidoximated silica. J. Radioanal. Nucl. Chem. 313, 113–121.

You, W., Peng, W., Tian, Z., Zheng, M., 2021. Uranium bioremediation with U(VI)-reducing bacteria. Sci. Total Environ. 798, 149107.

Yuan, Y., Liu, N., Dai, Y., Wang, B., Liu, Y., Chen, C., et al., 2020. Effective biosorption of uranium from aqueous solution by cyanobacterium Anabaena flos-aquae. Environ. Sci. Pollut. Res. 27, 44306–44313.

Zhang, X.-F., Ding, C.-L., Liu, H., Liu, L.-H., Zhao, C.-Q., 2011. Protective effects of ion-imprinted chitooligosaccharides as uranium-specific chelating agents against the cytotoxicity of depleted uranium in human kidney cells. Toxicology 286, 75–84.

Zhang, S., Shu, X.W., Zhou, Y., Huang, L., Hua, D.B., 2014. Highly efficient removal of uranium (VI) from aqueous solutions using poly(acrylic acid)-functionalized microspheres. Chem. Eng. J. 253, 55–62.

Zhang, B., Li, M., Zhang, X., Huang, J., 2016. Kinetics of uranium extraction from uranium tailings by oxidative leaching. JOM 68, 1990–2001.

Zhao, C.S., Liu, J., Deng, Y.H., Tian, Y.Y., Zhang, G.J., Liao, J.L., et al., 2019. Uranium(VI) adsorption from aqueous solutions by microorganism-graphene oxide composites via an immobilization approach. J. Clean. Prod. 236, 117624.

Zidan, I.H., Cheira, M.F., Bakry, A.R., Atia, B.M., 2020. Potentiality of uranium recovery from g.Gattar leach liquor using duolite ES-467 chelating resin: kinetic, thermodynamic and isotherm features. Int. J. Environ. Anal. Chem., 1748613 https://doi.org/10.1080/03067319.2020.1748613 In press.